



# Analysis of radiative opacities for optically thin and thick astrophysical plasmas

Guadalupe Espinosa, Rafael Rodríguez\*, Juan Miguel Gil

IUNAT, Departamento de Física, Universidad de Las Palmas de Gran Canaria, Las Palmas de Gran Canaria, 35017, Spain



## ARTICLE INFO

### Article history:

Received 13 July 2019

Revised 29 August 2019

Accepted 29 August 2019

Available online 5 September 2019

### Keywords:

Monochromatic and multigroup opacities

Non-local thermodynamic equilibrium

Plasma self-absorption

Astrophysical plasmas

## ABSTRACT

The resolution of the radiative transfer equation in radiation-hydrodynamic simulations of astrophysical plasmas require radiative opacities. In this work, an analysis of the monochromatic and multigroup opacities of an astrophysical plasma mixture has been carried out. The study has been made in ranges of electron temperatures and densities of  $1 - 1000$  eV and  $10^{11} - 10^{20} \text{ cm}^{-3}$ , respectively, a wide range of plasma conditions that can be found in several astrophysical scenarios where local and non-local thermodynamic regimes are attained. Collisional-radiative calculations were performed to obtain the plasma level populations and the monochromatic opacities in that range of plasma conditions, covering both thermodynamic regimes. Since the astrophysical mixture includes chemical elements from hydrogen to iron, their contribution to the total opacity will depend on the plasma conditions and we have made a characterization of their contribution as a function of the electron density and temperature and also of the photon frequency. Multigroup and gray approaches are commonly used in the radiative transfer equation in radiation-hydrodynamic calculations. We have analyzed the influence of the number of the groups in the accuracy of the multigroup opacities and we have showed that, for a given plasma condition, the opacity of the multicomponent plasma in the gray approach may be considerably influenced by only some of the contributing elements, due to the influence of the weighting function in the mean, which can lead to great differences with respect to the monochromatic opacity. Finally, since there are situations in which the self-absorption of the plasma radiation becomes relevant due to the dimensions of the plasma, we have performed an analysis of the influence of the radiation trapping in the monochromatic and multigroup opacities in terms of the plasma conditions and the width of the plasma slab, assuming the plasma with planar geometry and we have also studied the departures of the local thermodynamic regime.

© 2019 Elsevier Ltd. All rights reserved.

## 1. Introduction

Radiative opacities play a key role in plasmas in astrophysics scenarios. Thus, for example, the opacities of stellar mixtures are responsible for the energy transfer in the stars which has an impact in the stellar structure and evolution [1] and pulsation [2], they rule the levitation of metals in the stellar interiors [3] and they are also important in radiative shocks in optically thick media [4]. Furthermore, radiation hydrodynamic simulations of astrophysical flows require of opacities due to the coupling between hydrodynamic or magneto-hydrodynamic and radiative transfer equations.

The radiative quantities of particular interest in radiation hydrodynamic simulations are the radiative energy density, flux and

pressure tensor, which involve integrals of specific intensity over the frequency variable [5]. This fact justifies to integrate the equation of transfer over frequency and the use of frequency-averaged radiative opacities. On the contrary, when solving the radiative transfer equation the use of a mean opacity approach that averages over the whole spectrum might be too crude. However, the direct method based on the use of detailed opacities, that include a large number of frequency points in order to represent all the major features of the opacities, frequently involves considerably long computational times, overall for complex spectra and when the radiative transfer equation is coupled to hydrodynamic simulations. A widely accepted approach for handling the frequency variable in the equation of transfer is the multigroup method [6]. In this approach, the opacity spectrum is divided into a number of frequency groups, each of which spans a definite range. Within each group, the radiative opacity is replaced by its weighted integrals over the group. Planck or Rosseland means are generally used

\* Corresponding author.

E-mail address: [rafael.rodriguezperez@ulpgc.es](mailto:rafael.rodriguezperez@ulpgc.es) (R. Rodríguez).

in the multigroup method. This method is preferable to the one-group method, or gray approach, since as the number of groups increases the frequency-averages of the opacity are less sensitive to the weighting function used in computing these averages and, therefore, a relatively crude estimate for the specific intensity will lead to more accurate results in the former method than in the latter one [6].

Much effort has been devoted in the calculation of radiative opacities of astrophysical plasmas in the local thermodynamic equilibrium (LTE) regime approach [7–13]. LTE regime is attained in plasmas whose dimensions are considerably smaller than the photon mean free paths but are rather longer than the collision length between ions and electrons [14]. Low electron temperatures and high densities encourage the LTE thermodynamic regime. However, in many situations, the plasma conditions are such the LTE requirements are not fulfilled and, then, the plasmas are in non-LTE (NLTE) regime. In this case, the radiative opacities may differ substantially from those obtained assuming the plasma to be in LTE. The calculations of the radiative opacities, which depend on the atomic level populations, are much more complicated in NLTE than in LTE. Most of the NLTE simulations are based in the so-called collisional-radiative (CR) models [15]. In these models the distribution of the atomic level populations are obtained solving large sets of coupled rate equations which include atomic processes that couple photons, free electrons and atomic states. Two issues are critical in NLTE simulations. The first one is the degree of the atomic description. For low-Z atoms it is feasible to use fine structure descriptions. However, as the atomic number increases these descriptions become intractable since the number of levels increases exponentially [16]. In this situation, the statistical approaches based on grouping levels into configurations, such as the detailed configuration account (DCA) combined with the unresolved transition array (UTA) formalism [17], or grouping configurations into superconfigurations together with the supertransition array formalism [18] have proved their suitability. When a more detailed description of the spectrum is needed, as for example for spectroscopic purposes, hybrid methods, that mix fine description for the relevant transitions and these statistical approaches for the others, have been developed [19,20]. The second issue is the question of which and how many atomic levels should be included in the CR model, i.e. the problem of the atomic-space completeness. Since its achievement is very difficult or even impossible [21], the choice of the atomic-state has to be done carefully and will be determined by the conditions of the plasma under analysis. For instance, for photoionized plasmas, atomic configurations that include inner shells open should be included. On the other hand, for moderate plasma densities in which the ionization is mainly due to collisions with thermal electrons the number of configurations can be restricted [21].

In a previous work [22], we presented an analysis of the NLTE effects in the simulations of Rosseland and Planck mean opacities for an astrophysical plasma mixture in ranges of electron temperatures and densities 1–1000 eV and  $10^{11} - 10^{20} \text{ cm}^{-3}$ , respectively, which is a wide range of plasma conditions where LTE and NLTE regimes are attained and that can be found in several astrophysical scenarios [23–26]. The chemical elements considered in the plasma mixture were H, He, C, N, O, Ne, Na, Mg, Al, Si, S, Ar, Ca and Fe and solarlike abundances [27] were taken for them. In the present work, we present an study of monochromatic and multigroup opacities for this plasma mixture in that range of plasma conditions. In the mixture, there are chemical elements with atomic number from 1 to 26, which implies very different ionization potentials and electronic configurations. Therefore, their contribution to the total opacity could be quite different as a function of the electron density and temperature and also in the range of photon energies. As far as we know, there is a lack of systematic

study of the contribution of the different chemical elements to the monochromatic opacity of the mixture in the range of plasma conditions considered in this work, that include NLTE and LTE regimes. We also study the one and multigroup approaches for the opacity of the mixture focusing in the influence of the number of groups included. These analysis are done assuming the plasma as optically thin, i.e. without including external radiation fields or plasma self-absorption. However, in many situations the plasma optical depth can lead to situations in which the radiation trapping can modify noticeably the microscopic properties of the plasma and, in particular, its opacity. We have also carried out an analysis of the influence of the optical depth in the opacity with respect to the optically thin situation and also we have study the departures from LTE regime as a function of the plasma conditions. This study is made both for the monochromatic and multigroup and one group opacities.

The paper is structured as follows. In the next section, the theoretical model and computational codes used in this work to simulate the plasma atomic level populations and monochromatic and multigroup opacities are presented. Section 3 is devoted to the results obtained and this is divided into three sub-sections. Sections 3.1 and 3.2 are dedicated to the analysis of the monochromatic and multigroup opacities, respectively, assuming the multi-component plasma as optically thin. In Section 3.3, the analysis of the influence of the plasma self-absorption in the monochromatic and multigroup opacities of the plasma mixture is addressed. Finally, Section 4 summarizes the results and the main conclusions.

## 2. Theoretical model

### 2.1. Atomic properties

The energy levels, wave functions, oscillator strengths and photoionization cross sections used in the present CRSS model were calculated using the FAC code [28]. In this code, a fully relativistic approach based on the Dirac equation is used and the atomic levels of an atomic ion are obtained by diagonalizing the relativistic Hamiltonian. These atomic data were obtained on the relativistic detailed configuration (RDCA) accounting approach. The radiative transitions rates in FAC are calculated in the single multipole approximation, and in this work they were obtained in the electric dipole approach. In the RDCA approach, the oscillator strengths provided by the FAC code include configuration interaction effects due to the mix between relativistic configurations that belong to the same non-relativistic one.

With regard to the choice of atomic configurations, we have included those with an energy within two times the ionization energy of the ground configuration. For the kind of plasmas studied in this work, in which external radiation fields or hot electrons are not present, and for the wide range of plasma conditions analyzed, this criterion to select the configurations ensures that the most relevant configurations are included in the whole range of conditions [13,22], what is sufficient for the qualitatively study performed in this work.

### 2.2. Plasma level populations

As said before, in the NLTE regime plasma level populations are obtained solving the rate equations of the CR models, which are given by

$$\frac{dN_{\zeta i}(\mathbf{r}, t)}{dt} = \sum_{\zeta' j} N_{\zeta' j}(\mathbf{r}, t) R_{\zeta' j \rightarrow \zeta i}^+ - \sum_{\zeta' j} N_{\zeta i}(\mathbf{r}, t) R_{\zeta i \rightarrow \zeta' j}^- \quad (1)$$

where  $N_{\zeta i}$  is the population density of the atomic level  $i$  of the ion with charge state  $\zeta$ . The terms  $R_{\zeta' j \rightarrow \zeta i}^+$  and  $R_{\zeta i \rightarrow \zeta' j}^-$  take into

account all the atomic processes, both collisional and radiative, which contribute to populate and depopulate the atomic configuration  $\zeta i$ , respectively. These atomic processes are responsible for the atomic level populations distribution in the plasma. Two complementary equations have to be satisfied together with (1). First, the requirement that the sum of all the partial densities equals the total ion density,  $n_{ion}$ ,

$$\sum_{\zeta=0}^Z \sum_{i=0}^{M_{\zeta}-1} N_{\zeta i} = n_{ion}, \quad (2)$$

and, second, the charge neutrality condition in the plasma,

$$\sum_{\zeta=0}^Z \sum_{i=0}^{M_{\zeta}-1} \zeta N_{\zeta i} = n_e, \quad (3)$$

where  $M_{\zeta}$  is the total number of levels for the charge state  $\zeta$  and  $n_e$  the electron density. The plasma average ionization is defined as

$$\bar{Z} = \frac{\sum_{\zeta=0}^Z \zeta N_{\zeta}}{\sum_{\zeta=0}^Z N_{\zeta}} = \frac{n_e}{n_{ion}}. \quad (4)$$

For a given condition of density and temperature, the resolution of the rate equations also provides the plasma charge state distribution (CSD) which is defined as the set of the population densities,  $\{N_{\zeta}\}$ , of the ions present in the plasma.

For optically thick plasmas, since radiation induced processes are included in the CR model, the rate equations are coupled to the radiative transfer equation (RTE), which is given by

$$\frac{1}{c} \frac{\partial I_{\nu}(\mathbf{r}, t, \nu, \mathbf{n})}{\partial t} + \mathbf{n} \cdot \nabla I_{\nu}(\mathbf{r}, t, \nu, \mathbf{n}) = j(\mathbf{r}, t, \nu) - \kappa(\mathbf{r}, t, \nu) I_{\nu}(\mathbf{r}, t, \nu, \mathbf{n}), \quad (5)$$

where  $\nu$  is the photon frequency,  $\mathbf{n}$  is a unit vector in the direction of propagation for any value of the solid angle,  $I_{\nu}(\mathbf{r}, t, \nu, \mathbf{n})$  is the specific intensity and  $j(\mathbf{r}, t, \nu)$  and  $\kappa(\mathbf{r}, t, \nu)$  are the plasma monochromatic emissivity and absorption coefficients, i.e. the plasma radiative properties, that we have assumed as isotropic, which is a common approximation. Taking into account that the source function is given by

$$S(\mathbf{r}, t, \nu) = \frac{j(\mathbf{r}, t, \nu)}{\kappa(\mathbf{r}, t, \nu)}, \quad (6)$$

Eq. (5) can be written as

$$\frac{1}{c} \frac{\partial I_{\nu}(\mathbf{r}, t, \nu, \mathbf{n})}{\partial t} + \mathbf{n} \cdot \nabla I_{\nu}(\mathbf{r}, t, \nu, \mathbf{n}) = \kappa(\mathbf{r}, t, \nu) [S(\mathbf{r}, t, \nu) - I_{\nu}(\mathbf{r}, t, \nu, \mathbf{n})]. \quad (7)$$

Both the source function and the absorption coefficient depend on the plasma level populations and, therefore, for optically thick situations (1) and (5) must be solved simultaneously and self-consistently. In the present work, the atomic level populations have been obtained assuming the plasma in steady-state. In this case, the time-derivative in the rate equations of the CR model (see (1)) vanishes, obtaining

$$\sum_{\zeta'j} N_{\zeta'j}(\mathbf{r}, t) R_{\zeta'j \rightarrow \zeta i}^+ - \sum_{\zeta'j} N_{\zeta i}(\mathbf{r}, t) R_{\zeta i \rightarrow \zeta'j}^- = 0. \quad (8)$$

In the following we will denote the CR model in the steady-state approach as CRSS model. This approach is valid when the characteristic time of the most relevant atomic process in the plasma is considerably shorter than the characteristic time of the plasma evolution (i.e. the time associated to changes in the plasma density and temperature). When this criterion is fulfilled, we could consider that the atomic processes are fast enough to distribute

the atomic level populations in the plasma before the density and temperature of the plasma change.

The CRSS model used in this work is implemented in MIXKIP code [22] and the atomic processes included are collisional ionization [29] and three-body recombination, spontaneous decay [28], collisional excitation [30] and deexcitation, radiative recombination [31], autoionization and electron capture [32]. The rates of the inverse processes are obtained through the detailed balance principle. A Maxwell-Boltzmann distribution is assumed for the free electrons when calculating the rates of the collisional atomic processes, which implies that the free electrons have thermalized. In a previous work [22], we presented calculations of the electron mean free paths for the plasma mixture and the range of conditions considered in this work, assuming the plasma as homogeneous in density and temperature and non-relativistic. These mean free paths provide estimations of the plasma average volume needed for the free electrons to thermalize. The mean free paths obtained ranged from  $10^{-7}$  to  $10^2$  m, decreasing with the electron density and increasing with the electron temperature, as expected. When substantial deviations from Maxwell-Boltzmann distributions are produced, due to the characteristic times and lengths of the plasma are lower than those required for the thermalization, the free electron energy distribution functions are usually obtained from a simultaneous solution of the time-dependent atomic rate equations and Boltzmann electron kinetics [33]. However, this kind of simulation is tractable for the study of particular situations but not for analysis performed in wide range of plasma conditions, as in this work. In this case, thermal distributions for the free electrons are commonly assumed. In [22] we also checked that exchange effects were not quite relevant and therefore the use of the Fermi-Dirac distribution for the free electrons was not necessary. In the present CRSS model it is assumed that the collision times between ions and electrons are short enough so the ions can be considered to be at rest.

In this work, we have also addressed the effect of the plasma radiation self-absorption or radiation trapping in the microscopic properties of the multicomponent plasma. External radiation fields have not been considered in the analysis. As said before, for optically thick situations the rate equations and the radiative transfer equations are coupled and they must be solved selfconsistently. In the present work, the radiation trapping is included in the rate equations using the escape factor formalism which circumvents the need to carry out simultaneous calculations of radiative transport and atomic physics and also uncouples the radiative transfer and rate equations. The escape factor represents an alternative method of writing the net rate of line emission and, as a result, it leads to an effective reduction of the Einstein spontaneous emission coefficient. In the present CRSS model, the technique described in [34] is adopted, assuming a uniform distribution for emitting atoms and isotropic emission, for the calculation of the escape factors for the three basic geometries, planar, cylindrical, and spherical. For a given line transition,  $\zeta j \rightarrow \zeta i$ , the escape factor is given by

$$\Lambda_{ji} = \int_0^{\infty} \phi_{ij}(\nu) \frac{1}{\tau_{ij}(\nu)} F[\tau_{ij}(\nu)] d\nu, \quad (9)$$

where  $\tau_{ij}(\nu) = \kappa_{\zeta i \rightarrow \zeta j}(\nu) L$  denotes the optical depth,  $L$  represents the characteristic plasma dimension, i.e., slab width, cylinder, or sphere radius and  $F[\tau_{ij}(\nu)]$  is a functional of the optical depth whose particular form depends on the considered geometry.

With respect to the effect of the plasma environment on the plasma level populations, the formulation developed by Stewart and Pyatt [35] for the depression of the ionization potential or continuum lowering (CL) was applied in this work, which can reduce the number of bound states available.

In the present work, comparisons with LTE simulations are also performed. In this thermodynamic regime, the ion abundances are

obtained in MIXKIP by solving the Saha equation

$$\frac{N_{\zeta+1}n_e}{N_{\zeta}} = \frac{Z_e Z_{\zeta+1}}{Z_{\zeta}} e^{-(I_{\zeta} - \Delta I_{\zeta})/kT_e}, \quad (10)$$

where  $T_e$  is the electron temperature,  $Z_e$  and  $Z_{\zeta}$  are the partition functions of free electrons and ion  $\zeta$ , respectively,  $I_{\zeta}$  is the ionization potential of the ionization stage  $\zeta$  and  $\Delta I_{\zeta}$  is the CL of the ionization potential due to the plasma environment. The atomic plasma level populations are then obtained assuming a Boltzmann distribution.

### 2.3. Monochromatic and multigroup opacities

The plasma radiative opacities are calculated with the RAPCAL code [36,37] which uses the abundances of the atomic configurations provided by the CRSS model. The monochromatic absorption coefficient will be denoted  $\kappa(\nu)$  where, for the sake of simplicity, we have omitted the dependence on the position and time. This coefficient includes the bound-bound, bound-free and free-free contributions

$$\kappa(\nu) = \kappa_{bb}(\nu) + \kappa_{bf}(\nu) + \kappa_{ff}(\nu). \quad (11)$$

The bound-bound contribution to the absorption is given by

$$\kappa_{bb}(\nu) = \sum_{\zeta} \sum_{i,j} \kappa_{\zeta i \rightarrow \zeta j}(\nu), \quad (12)$$

with

$$\kappa_{\zeta i \rightarrow \zeta j}(\nu) = \frac{h\nu}{4\pi} N_{\zeta i} \frac{g_{\zeta j}}{g_{\zeta i}} \frac{c^2 A_{\zeta j \rightarrow \zeta i} \phi_{ij}(\nu)}{2h\nu_{ij}^3} \left( 1 - \frac{g_{\zeta i}}{g_{\zeta j}} \frac{N_{\zeta j}}{N_{\zeta i}} \right), \quad (13)$$

where  $h$  is the Planck's constant,  $c$  is the speed of light,  $g_{\zeta i}$  and  $g_{\zeta j}$  are the statistical weights of the  $i$  and  $j$  relativistic configurations, respectively. In the previous equation,  $\phi_{ij}(\nu)$  represents the line profile. In the evaluation of the line profile, natural, Doppler, electron-impact [38] and UTA broadenings [17] were included. The line-shape function is applied with the Voigt profile that incorporates all these broadenings.

The bound-free contribution to the absorption is given by

$$\kappa_{bf}(\nu) = \sum_{\zeta,i} \sum_{\zeta,j} \kappa_{\zeta i \rightarrow \zeta+1j}(\nu), \quad (14)$$

where

$$\kappa_{\zeta i \rightarrow \zeta+1j}(\nu) = N_{\zeta i} \sigma_{\zeta i \rightarrow \zeta+1j}^{pho}(\nu) \left( 1 - \frac{N_{\zeta+1j} n_e f(\varepsilon) g_{\zeta i}}{N_{\zeta i} g_{\zeta+1j} g(\varepsilon)} \right), \quad (15)$$

with  $\varepsilon$  the energy of the free electron,  $\sigma_{\zeta i \rightarrow \zeta+1j}^{pho}(\nu)$  the photoionization cross section,  $f(\varepsilon)$  the Maxwell-Boltzmann distribution and  $g(\varepsilon)$  the density of states with energy  $\varepsilon$  which is calculated in this work assuming an ideal gas of free electrons.

For the free-free contribution, the Kramers semi-classical expression for the inverse bremsstrahlung cross section has been used [39]

$$\sigma_{\zeta}^{ibr}(\nu) = \frac{16\pi^2 e^2 h^2 \alpha}{3\sqrt{3} (2\pi m_e)^{3/2}} \frac{\zeta^2 n_e}{T_e^{1/2} (h\nu)^3}, \quad (16)$$

and if a Maxwell-Boltzmann distribution is assumed for the free electrons, we obtain

$$\kappa_{ff}(\nu) = \frac{16\pi^2 e^2 h^2 \alpha}{3\sqrt{3} (2\pi m_e)^{3/2}} \frac{\overline{Z^2} n_{ion} n_e}{T_e^{1/2} (h\nu)^3} (1 - e^{-h\nu/T_e}). \quad (17)$$

where  $m_e$  and  $e$  are the electron mass and charge, respectively, and  $\alpha$  is the fine structure constant.

In order to determine the opacity,  $k(\nu)$ , the scattering of photons is also taken into account. In RAPCAL this one is approximated using the Thomson scattering cross section [40],  $\kappa_{scatt} = n_e \sigma^{Thom}$

with  $\sigma^{Thom} = 6.65 \times 10^{-25} \text{ cm}^2$ . Finally, the monochromatic opacity is given by

$$k(\nu) = \frac{1}{\rho} (\kappa(\nu) + \kappa_{scatt}), \quad (18)$$

with  $\rho$  the density of matter.

The group Planck,  $k_{p,g}$ , and Rosseland,  $k_{R,g}$  opacities are obtained from the monochromatic opacities [5], for a frequency range  $(\nu_g, \nu_{g+1})$ , as

$$k_{p,g} = \frac{\int_{\nu_g}^{\nu_{g+1}} B(\nu, T) (k(\nu) - \kappa_{scatt}/\rho) d\nu}{\int_{\nu_g}^{\nu_{g+1}} B(\nu, T) d\nu}, \quad (19)$$

$$\frac{1}{k_{R,g}} = \frac{\int_{\nu_g}^{\nu_{g+1}} \frac{1}{k(\nu)} \frac{\partial B(\nu, T)}{\partial T} d\nu}{\int_{\nu_g}^{\nu_{g+1}} \frac{\partial B(\nu, T)}{\partial T} d\nu}, \quad (20)$$

where  $B(\nu, T)$  is the Planckian function. For a single frequency group, they reduce to the mean opacities.

Finally, we would like point out that both MIXKIP and RAPCAL codes have been successfully tested with experimental results and numerical simulations for monocomponent plasmas of several elements included in the mixture analyzed in this work both in LTE and NLTE assumptions [36,37,41] and for the plasma mixture in LTE simulations [22].

## 3. Results

The results have been structured as follows. First, an analysis of the most relevant contributors to the monochromatic opacities as a function of the electron temperature and density is presented, assuming the plasma as optically thin. Subsequently, the effect of the plasma radiation trapping in the plasma atomic kinetics and monochromatic opacities is studied and comparisons with optically thin and LTE simulations are presented. Finally, this section ends with an analysis of the multigroup opacities. In this analysis we address the influence of the number of groups in their calculation and also the effect of the different atomic kinetic description used for their determination, e.g. optically thin and thick NLTE and LTE approaches.

### 3.1. Monochromatic opacities in optically thin situation

In the optically thin situation, the contribution of the different chemical elements of the mixture to the total opacity depends on the plasma conditions, i.e. the electron density and temperature, due to their different ionization potentials. Furthermore, they will also contribute in different parts of the photon energy range. In this work, we have carried out an analysis of the relevance of the contribution to the total opacity of the different chemical elements involved in the multicomponent plasma using the CRSS optically thin approach and for the whole range of plasma conditions considered in this work. To illustrate the results obtained in the analysis we have selected three densities,  $1.6 \times 10^{14}$ ,  $10^{17}$  and  $1.5 \times 10^{20} \text{ cm}^{-3}$ . The average ionizations and the CSDs of the elements do not change with the density for values lower than  $10^{14} \text{ cm}^{-3}$  so the conclusions obtained for this density can be extended to lower densities. On the other hand, the other two were chosen because they represent intermediate and large values of densities, respectively, in the range under consideration in this work. With respect to the temperature, we present results for 2, 10, 50, 100, 315, 630 and 1000 eV, thus covering the whole range of temperatures. The average ionization is more sensitive to the electron temperature than to the density and, for this reason, more cases are presented for the former. Furthermore, we have considered more cases in the range of temperatures 2–315 eV, where more variations in the average ionizations are detected, since for higher temperatures many



of the elements of the mixture are highly ionized. As the average ionization of the elements help to analyze their contributions to the absorption spectra, we have also represented that property, as a function of the electron density and temperature, along with the monochromatic opacities.

At the electron temperature of 2 eV and for the three densities under consideration the elements with a major contribution to the total monochromatic opacity are hydrogen, helium, carbon and oxygen, as Fig. 1 shows. Due to the different atomic structures of the ions involved, they will contribute in different ranges of photon energies as well. For the two lower densities, Fig. 1(a) and (b), the range of photon energies below 5 eV is dominated by the free-free contribution of the hydrogen and line transitions and photoionizations of its excited levels. For the photon energy range 5–10 eV we find a large contribution due to carbon line transitions, which presents a low average ionization (around 1, as Fig. 2(a) and (b) show) at this temperature and these two densities. For temperatures between 15–20 eV the spectrum is ruled by the photoionization of the ground state of hydrogen although some line transitions due to oxygen, whose average ionization is around 1 at both densities, are detected. In the range of photon energies 20–24 eV, the line and bound-free contributions of neutral helium dominate the monochromatic opacity (the average ionization for helium at both densities is around 0.3) whereas the  $\text{He}^{1+}$  ion dominates the spectra for higher photon energies. As the density increases, the hydrogen free-free contribution in the photon energies lower than 5 eV rises and this fact always occurs at any electron temperature. For the electron density of  $1.5 \times 10^{20} \text{ cm}^{-3}$  we detect a noticeable change in the spectra with respect to the other two densities represented, as Fig. 1(c) displays. Due to the increase of the recombination in the plasma, at this density the neutral ions are the most abundant ones for the chemical elements displayed. Therefore, as the abundance of hydrogen is considerably larger than that of the other elements, its line transitions are considerably stronger. Thus, the absorption spectrum is mainly ruled by hydrogen and to a lesser extent by helium. Furthermore, the line broadening due to collisional width is increased at this density and, therefore, the line overlapping is greater and a less detailed spectra is obtained than for the other two lower densities.

When the electron temperature increases to 10 eV, the average ionizations of the elements with lower atomic number present a more sensitive dependence with density than at the temperature of 2 eV. At the two lower densities analyzed, hydrogen is fully ionized and therefore its contribution to the opacity is only due to the free-free absorption in the range of photon energies lower than 5 eV. With respect to helium, we have obtained an average ionization for these two densities which is around 1.98. For this reason, and due to its great relative abundance, it presents a large contribution due to  $\text{He}^{+1}$  line transitions for photon energies between 40 and 60 eV and bound-free contribution for higher energies, as Fig. 3(a) and (b) show. At this temperature and for these densities, we also observe other low Z elements that contribute to the spectrum. Thus, besides carbon and oxygen, we also detect noticeable contributions due to nitrogen and neon, which relative abundances lower than the former ones. For these plasma conditions, the average ionizations for these four elements are quite similar and are around 3.5–4 (see Fig. 2 (a) and (b)). Due to their closeness in atomic number, they contribute to similar energy ranges in the spectra as Fig. 3(a) and (b) show (for clarity, we have not plotted the carbon contribution). Due to the greater abundance of oxygen, its contribution is more noticeable in general, although some structures associated with nitrogen and neon can also be observed in the figures. Chemical elements of the mixture with high atomic number present a smaller contribution although, for example, silicon and sulfur are responsible for most of the features observed for photon energies greater than 120 eV. Both figures also show

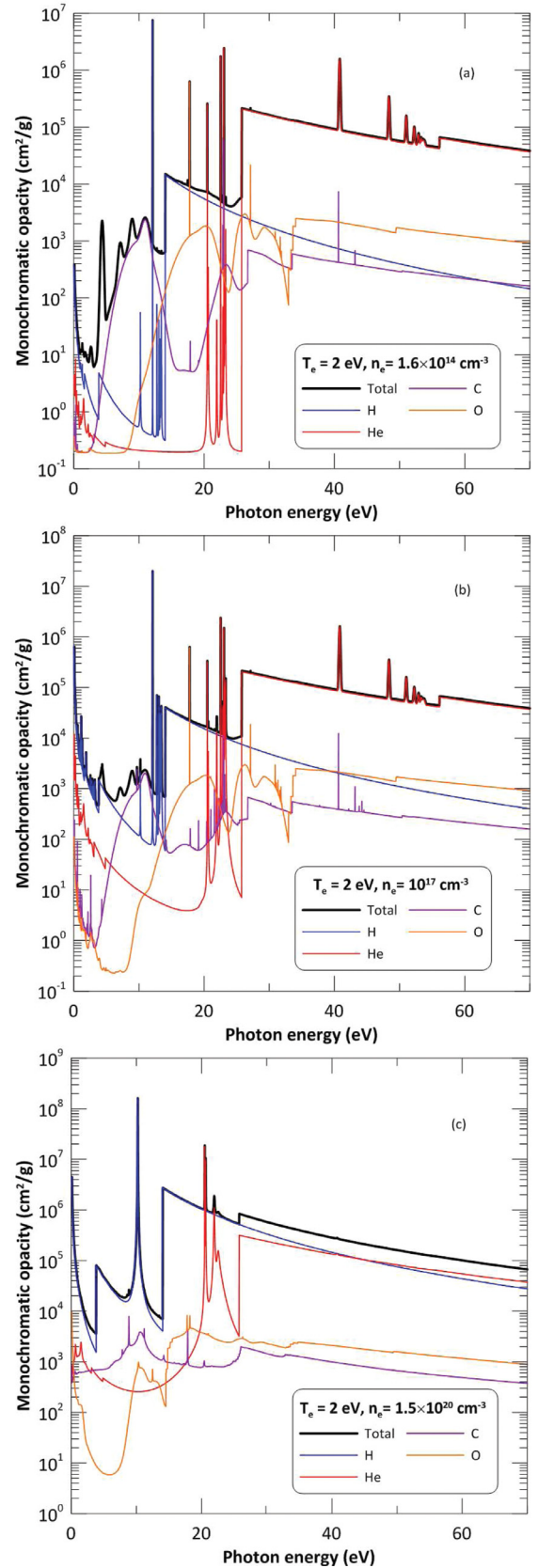
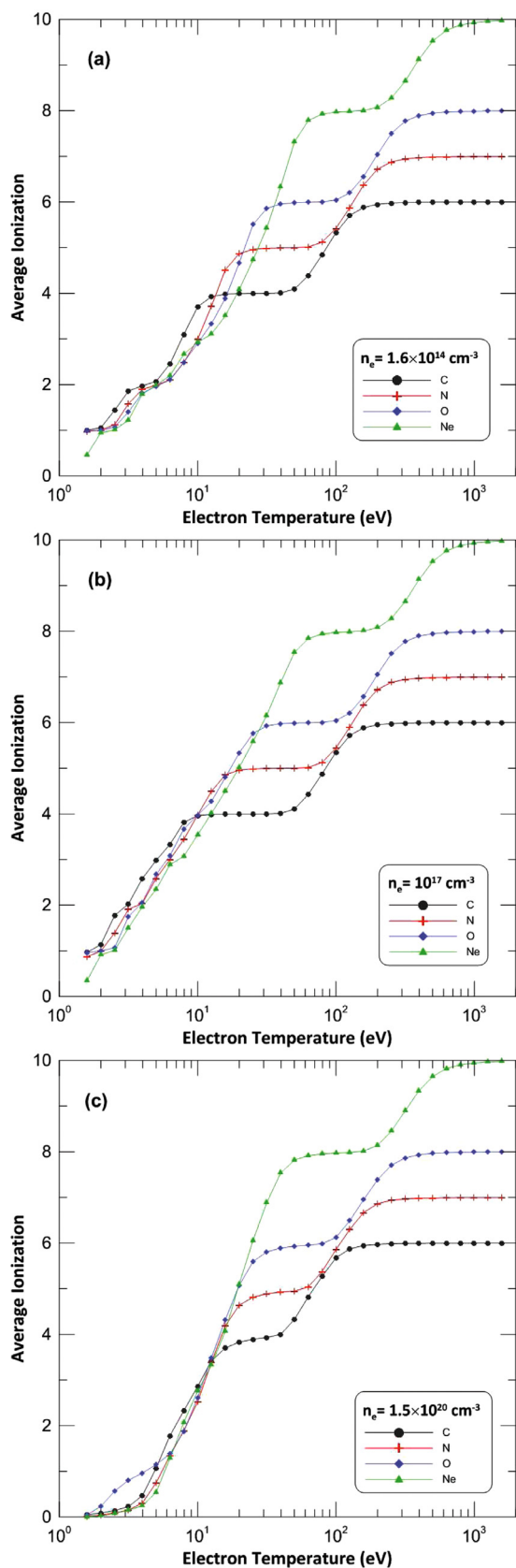
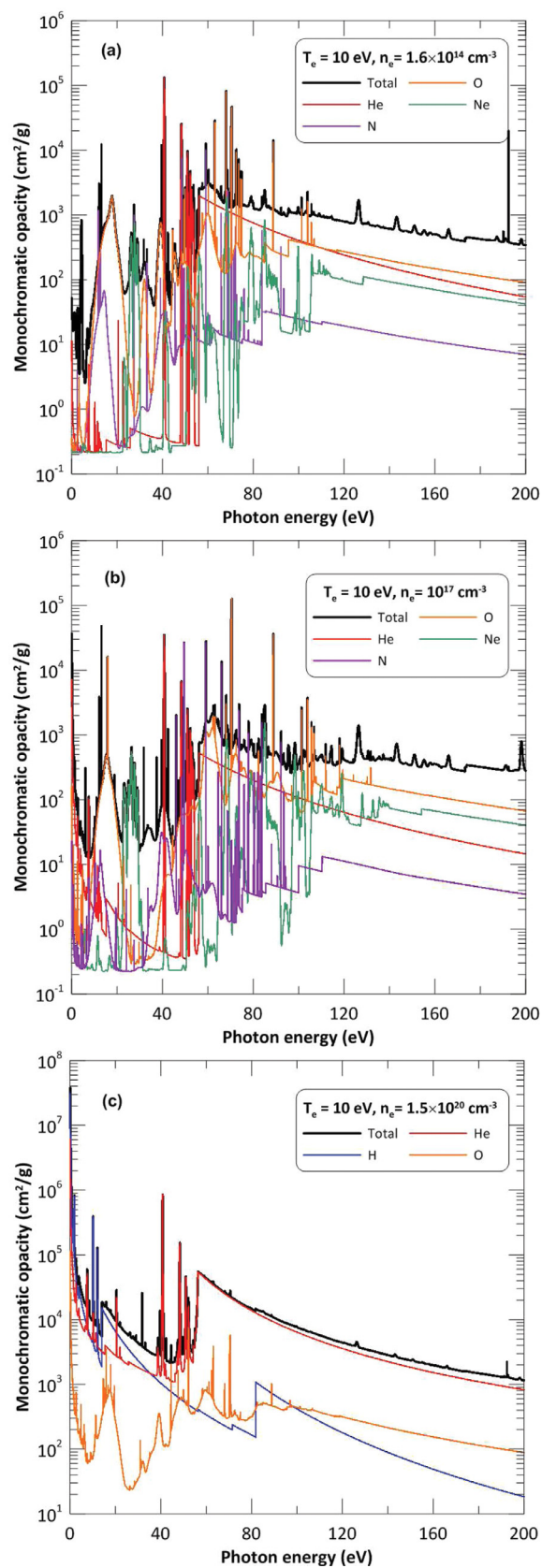


Fig. 1. Monochromatic opacities of the mixture and the contribution due to some relevant chemical elements, calculated at an electron temperature of 2 eV and for three electron densities: (a)  $1.6 \times 10^{14}$ , (b)  $10^{17}$  and (c)  $1.5 \times 10^{20} \text{ cm}^{-3}$ .



**Fig. 2.** Average ionization for C, N, O and Ne as a function of the electron temperature and for three electron densities: (a)  $1.6 \times 10^{14}$ , (b)  $10^{17}$  and (c)  $1.5 \times 10^{20} \text{ cm}^{-3}$ .



**Fig. 3.** Monochromatic opacities of the mixture and the contribution due to some relevant chemical elements, calculated at an electron temperature of 10 eV for three electron densities: (a)  $1.6 \times 10^{14}$ , (b)  $10^{17}$  and (c)  $1.5 \times 10^{20} \text{ cm}^{-3}$ .

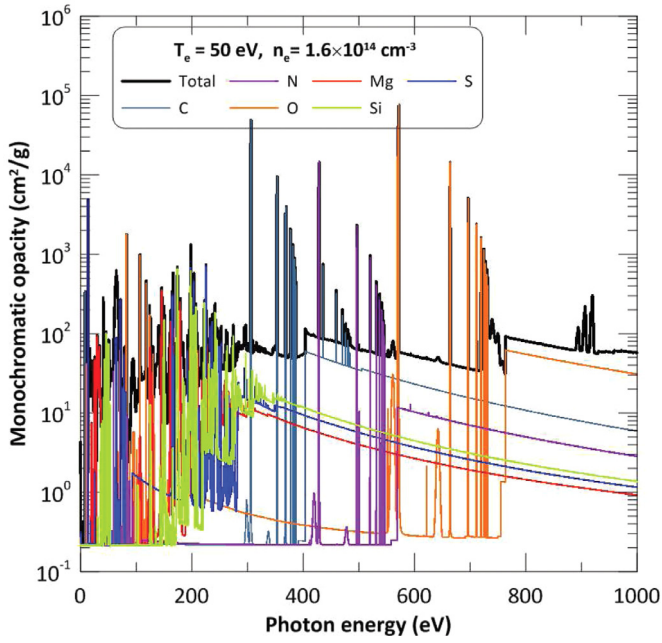


**Fig. 4.** Monochromatic opacities of the mixture and the contribution due to some relevant chemical elements, calculated at an electron temperature of 50 eV and electron density of  $1.6 \times 10^{14} \text{ cm}^{-3}$ .

an increase in the number of the line transitions in nitrogen and oxygen for the density of  $10^{17} \text{ cm}^{-3}$  with respect to the density of  $1.6 \times 10^{14} \text{ cm}^{-3}$ . This increase of density causes a rise in the population of excited levels due to a higher rate of collisional excitations and this could explain that issue. On the other hand, for the density of  $1.5 \times 10^{20} \text{ cm}^{-3}$ , the plasma recombination produces a decrease in the average ionizations of hydrogen and helium to values around 0.97 and 1.48, respectively. This fact along with their considerably large abundances cause the absorption to be ruled by these two elements, as for the same density at the electron temperature of 2 eV. This fact is well illustrated in Fig. 3(c) where we have added the contribution of oxygen in order to compare the three contributions.

When the electron temperature increases to 50 eV, the relevance of hydrogen and helium contributions become less important since they are fully ionized. On the other hand, in addition to the group of elements C-Ne, which was already important at 10 eV, we find other elements that have noticeable contributions to the opacity, which are magnesium, silicon and sulfur, as Fig. 4 shows. With respect to the group of elements C-Ne, their average ionizations for this temperature and for the three densities under analysis are located in a plateau associated with the electronic configuration of the He-like ion (see Fig. 2). Thus, their contributions to the opacity are grouped in two ranges of photon energies. The first ones, energies lower than 200 eV, mainly associated with the contributions due to the Be-like and Li-like ions, and the second ones for energies greater than 200, 400 and 600 eV for carbon, nitrogen and oxygen, respectively, corresponding to the contributions due to the He-like and H-like ions. Although for clarity we have not plotted the absorption spectrum for neon, this contributes in the range of energies lower than 250 eV and is responsible for the peaks obtained around the photon energies of 900 eV. With respect to magnesium, silicon and sulfur, as Fig. 5 shows, their average ionizations range from around 6.2 to 8.7, for the lower and greater densities, respectively. Therefore, the most abundant ions are those with ground configurations of the type  $1s^2 2(s, p)^k$ , with  $k$  the total number of electrons in the  $n = 2$  shell, for the three densities considered and their line contributions are mainly located for pho-

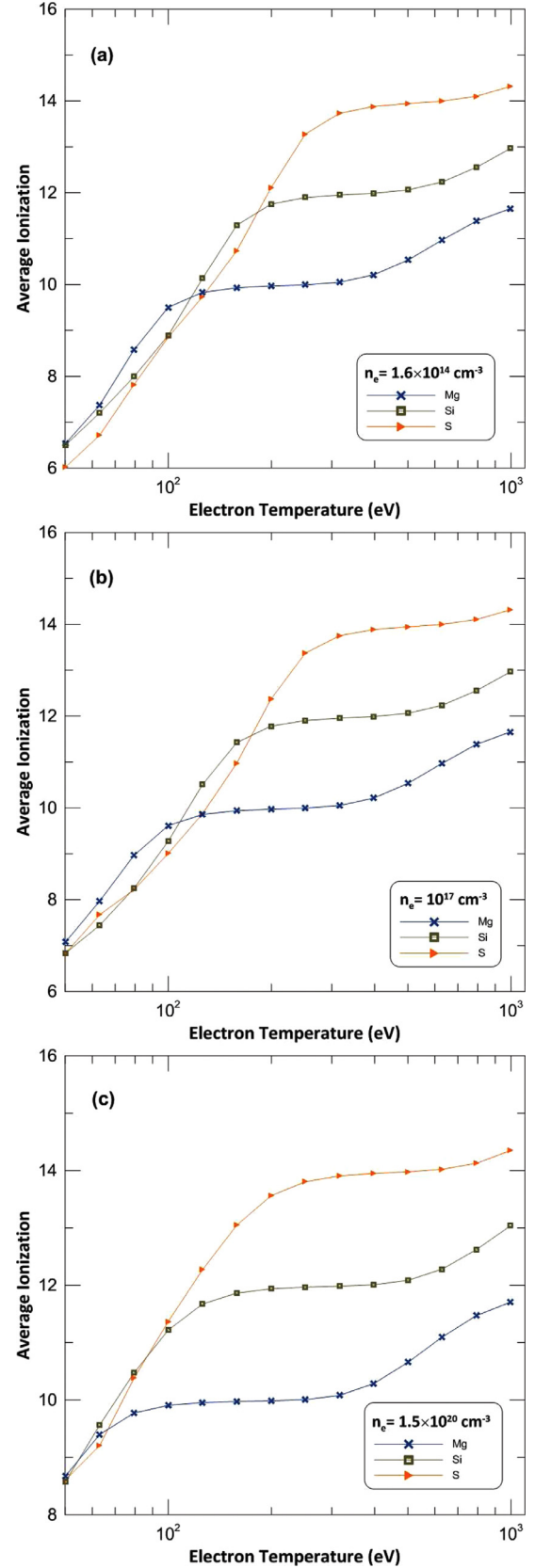


**Fig. 5.** Average ionization for Mg, Si and S as a function of the electron temperature and for three electron densities: (a)  $1.6 \times 10^{14}$ , (b)  $10^{17}$  and (c)  $1.5 \times 10^{20} \text{ cm}^{-3}$ .



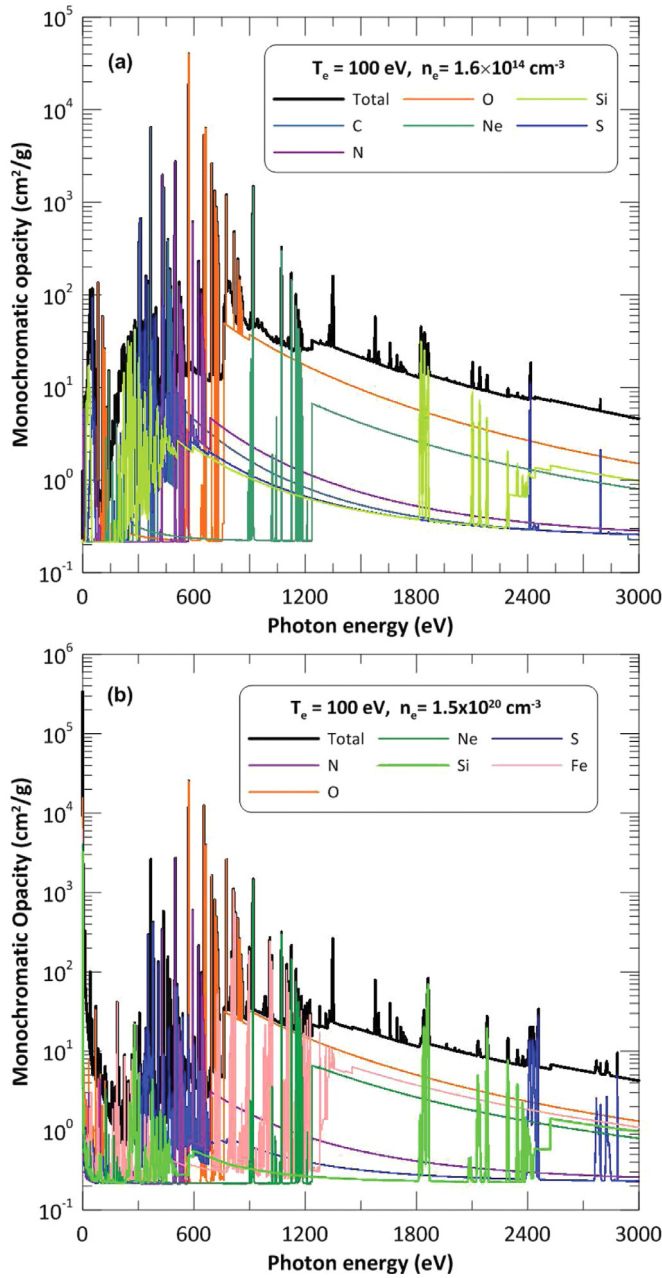


**Fig. 6.** Monochromatic opacities of the mixture and the contribution due to some relevant chemical elements, calculated at an electron temperature of 100 eV and electron densities of (a)  $1.6 \times 10^{14}$  and (b)  $1.5 \times 10^{20}$  cm⁻³.

ton energies lower than 400 eV for the three conditions as well. This result and the fact that the average ionizations of the C-Ne group do not change with the density at this temperature, make that their contributions to the absorption spectra are quite similar for the three densities considered. For this reason we have only represented the simulations for one density.

At the electron temperature of 100 eV, the average ionization of oxygen and neon are still in the plateau of the He-like ion for the three densities and, therefore, their contributions to the opacity are quite similar to those obtained at the temperature of 50 eV. Something similar occurs for carbon and nitrogen since, although the average ionization, which is around 5.5 for both elements, is slightly greater than at 50 eV, the ions that contribute at this temperature are the same that at 50 eV. On the other hand, the changes in the average ionizations of the group Mg-Si-S are more notice-

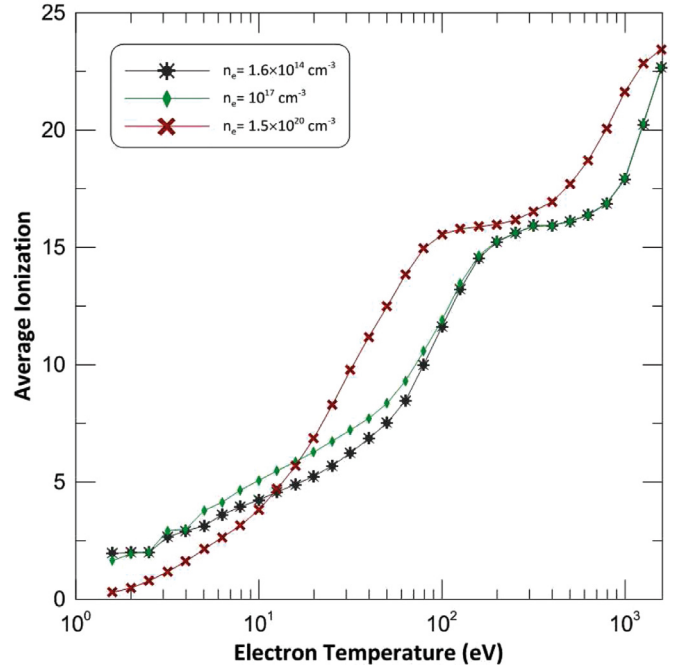


**Fig. 7.** Average ionization for Fe as a function of the electron temperature and for three electron densities: (a)  $1.6 \times 10^{14}$ , (b)  $10^{17}$  and (c)  $1.5 \times 10^{20}$  cm⁻³.

able. Thus, the average ionization of magnesium is ranged from 9 to 10, for the lowest and largest densities represented respectively, whereas for silicon and sulfur this is between 8 and 11.2. The most abundant ions involved at this temperature have the same kind of atomic configurations as at 50 eV but with a significantly lesser number of bound electrons. Therefore, their contributions are shifted to higher photon energies than at 50 eV, as Fig. 6 (a) and (b) show.

At this temperature, the iron starts contributing substantially, although primarily for the high density range. The average ionization of iron at this temperature is ranged from 12 to 16, as Fig. 7 shows. For the lower density, the ground configurations of the most abundant iron ions are of the type  $1s^2 2(s, p)^8 3(s, p)^k$  and their contribution are mainly located on a region of photon energies (lower than 600 eV) where the silicon contribution is significantly stronger. However, for the largest density, the increase of the silicon average ionization leads to a reduction of its contribution in this range and then the iron contribution can be detected. Furthermore, the increase of the iron average ionization with the density, which is around 16, implies the presence of ions with ground configurations like  $1s^2 2s^2 2p^k$ , which contributes to the total spectrum at photon energies greater than 600 eV.

As the temperature increases, the type of ions of the C-Ne group which are present in the mixture are the same (mainly, the H-like and the fully stripped ones) and, therefore, their contributions to the total spectrum remain quite similar for temperatures greater than or equal to 300 eV. An analogous situation is found for the elements of the group Mg-Si-S, although, in this case, the ions involved are less charged than the previous group of elements, mainly the Li-like, He-like and H-like ones. These issues are illustrated in Figs. 8 and 9, where the contributions of several of these elements to the total spectra are represented at two electron temperatures, 630 and 1000 eV, respectively, and for electron densities of  $1.6 \times 10^{14}$  and  $1.5 \times 10^{20}$  cm⁻³. The He-like and H-like transitions of the Mg-Si-S group are detected in the range of photon energies around 1600–3400 eV. Calcium and argon has lower abundances but some peaks associated to them are detected in the spectra. In particular, the peaks observed around the photon ener-



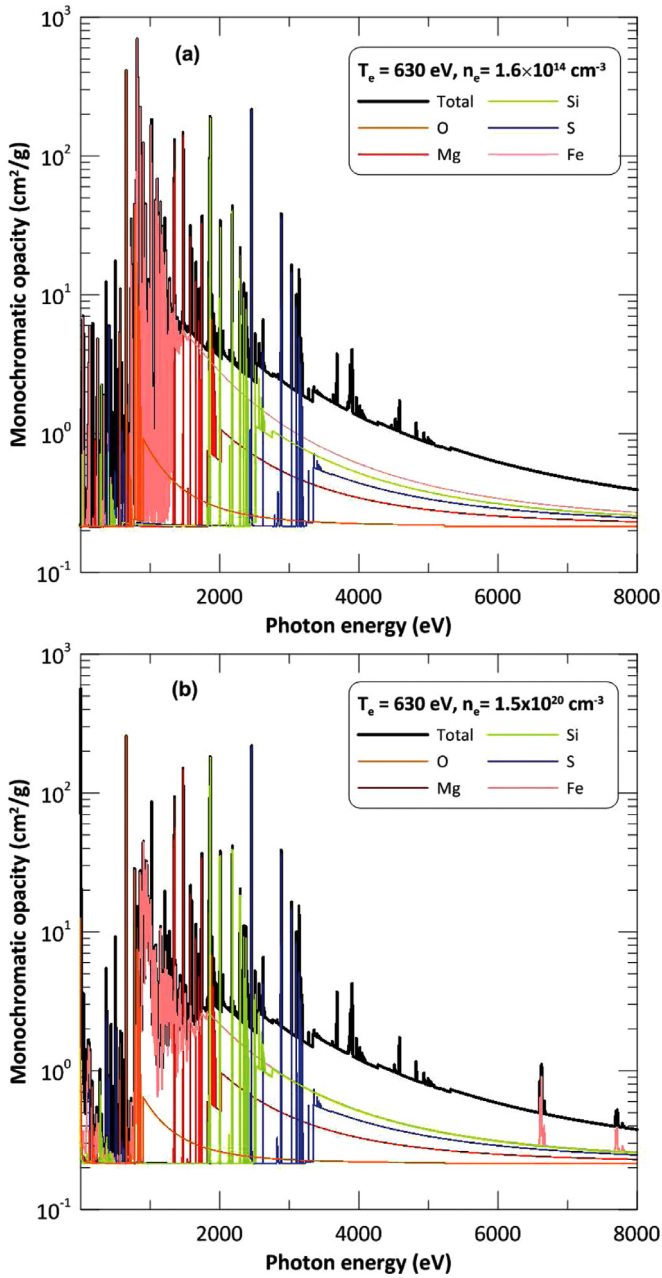


**Fig. 8.** Monochromatic opacities of the mixture and the contribution due to some relevant chemical elements, calculated at an electron temperature of 630 eV and for two electron densities: (a)  $1.6 \times 10^{14}$  and (b)  $1.5 \times 10^{20} \text{ cm}^{-3}$ .

gies of 4000 eV are associated to both elements and those around 4500–5000 eV to transitions of calcium ions.

At these two electron temperatures, the iron contribution to the spectra is noticeable. At the temperature of 630 eV and density of  $1.6 \times 10^{14}$  the most abundant ions are  $\text{Fe}^{16+}$  and  $\text{Fe}^{17+}$ , which ground atomic configurations  $2p^6$  and  $2p^5$ , respectively. Line contributions of these ions are mainly located in the range of photon energies between 600 and 2000 eV. The increase of the electron density to  $1.5 \times 10^{20} \text{ cm}^{-3}$  yields an increase in average ionization and the ions ranging from  $\text{Fe}^{17+}$  to  $\text{Fe}^{20+}$  becomes more relevant. They have electronic configurations of  $2p^5$  to  $2p^2$  and their contributions are in the same region of photon energies as for case of lower density. However, at this high density the abundance of the He-like Fe ion begins to be more appreciable and, as a consequence, some features are detected for photon energies between

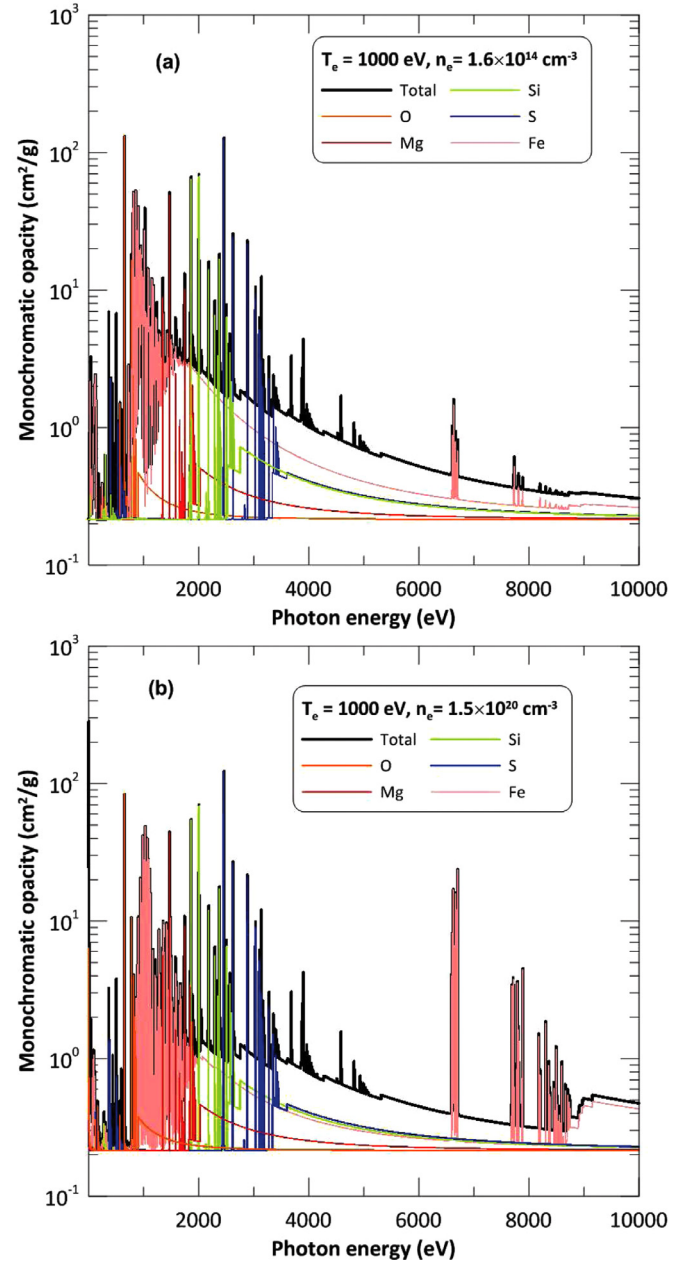


**Fig. 9.** Monochromatic opacities of the mixture and the contribution due to some relevant chemical elements, calculated at an electron temperature of 1000 eV and for two electron densities: (a)  $1.6 \times 10^{14}$  and (b)  $1.5 \times 10^{20} \text{ cm}^{-3}$ .

6000–8000 eV, as Fig. 8(b) shows. When the temperature is increased to 1000 eV, these structures are observed at the electron density of  $1.6 \times 10^{14} \text{ cm}^{-3}$  (see Fig. 9(a)) since the iron average ionization at this condition is quite close to that at the temperature of 630 eV and density of  $1.5 \times 10^{20} \text{ cm}^{-3}$ . The contributions due to the He-like Fe ion is considerably increased at this last density for the electron temperature of 1000 eV, since the average ionization in this case is around 22 (ground configuration  $1s^2 2s^2$ ) as Fig. 7 shows, which enhances the abundance of this ion and also the abundance of the H-like Fe ion which is the responsible of the peaks observed at photon energies greater than 8000 eV.

### 3.2. Multigroup opacities in optically thin situation

As said before, the multigroup method is a commonly used method for handling the frequency variables in the RTE in order to

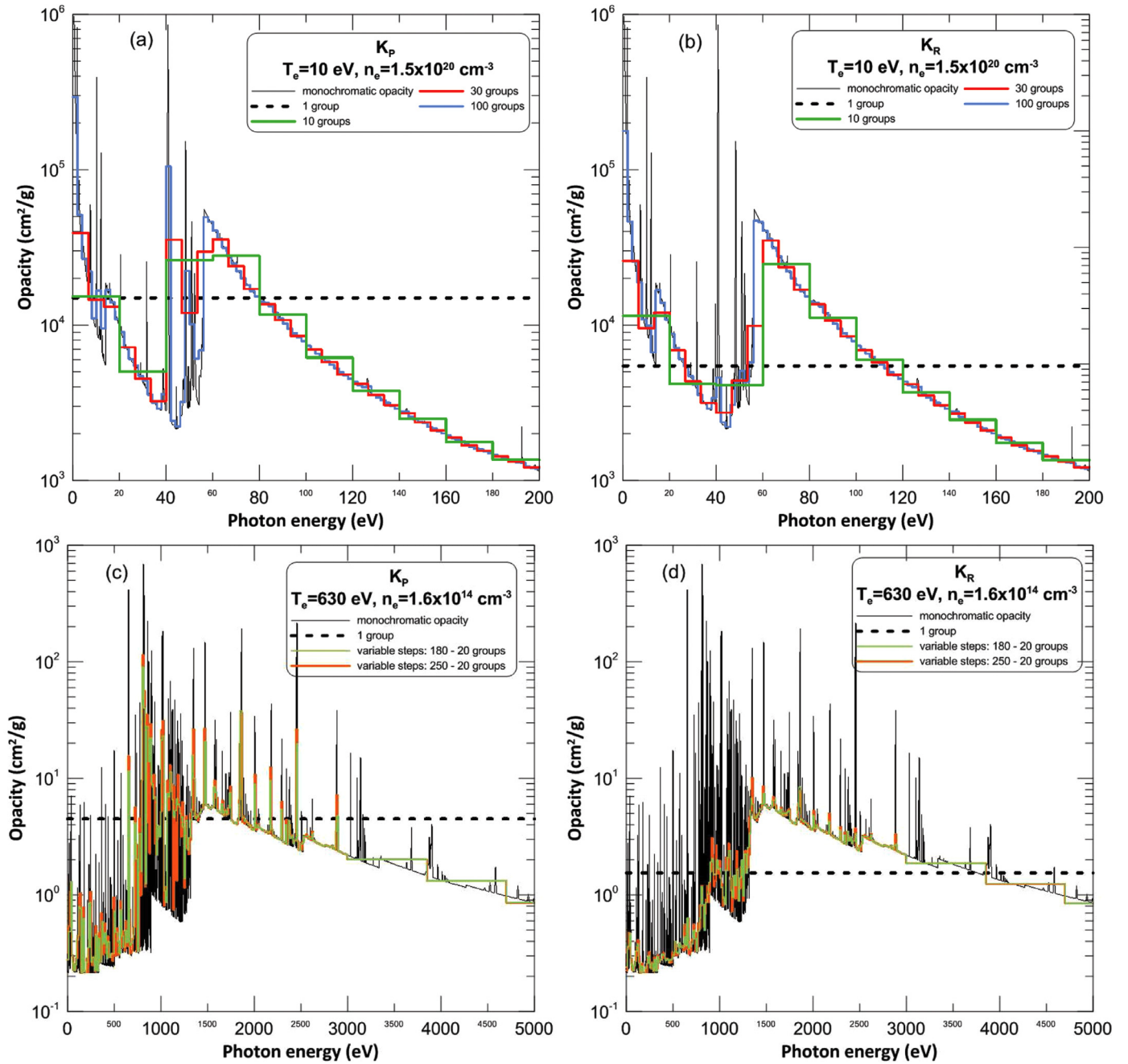


**Fig. 10.** Comparison of the monochromatic opacities and group Planck and Rosseland mean opacities calculated at two plasma conditions and with different number of groups.

achieve a compromise between accuracy and computational costs. If we divide the frequency range into  $M$  groups and we integrate (7) in frequency over the  $g$ th group then we have

$$\frac{1}{c} \frac{\partial I_g(\mathbf{r}, t, \nu, \mathbf{n})}{\partial t} + \mathbf{n} \cdot \nabla I_g(\mathbf{r}, t, \nu, \mathbf{n}) = \kappa_g(\mathbf{r}, t, \nu, \mathbf{n}) [S_g(\mathbf{r}, t, \nu) - I_g(\mathbf{r}, t, \nu, \mathbf{n})] \quad (21)$$

where the mean absorption coefficient is given by

$$\kappa_g(\mathbf{r}, t, \nu, \mathbf{n}) = \frac{\int_{\nu_g}^{\nu_{g+1}} \kappa(\nu) [S_g(\mathbf{r}, t, \nu) - I_g(\mathbf{r}, t, \nu, \mathbf{n})] d\nu}{\int_{\nu_g}^{\nu_{g+1}} [S_g(\mathbf{r}, t, \nu) - I_g(\mathbf{r}, t, \nu, \mathbf{n})] d\nu}. \quad (22)$$

From the equation we observe that the mean absorption coefficient includes angular dependence through the specific intensity. Furthermore, the calculation of the coefficient involves the specific in-

tensity, which is unknown. In the multigroup method the assumption is that the mean absorption coefficient is relatively independent to the weighting function. On the other hand, since the radiative opacities are, in general, widely varying functions of frequency, a low number of groups included in the multigroup method will cause an increase of the influence of the weighting function. In practice,  $\kappa_g(\mathbf{r}, t, \nu, \mathbf{n})$  is usually taken as either a Planck group opacity, given by (19) and where the Planck function is used as weighting function, or Rosseland group opacity, given by (20) and which follows from the assumption of the equilibrium diffusion approximation for the specific intensity.

We have performed an study of the influence of the number of the groups in the group opacity mean for the plasma mixture. Figs. 10(a) and (b) display a comparison of the monochromatic

opacities and group Planck and Rosseland and mean opacities, respectively, for an electron temperature of 10 eV and electron density of  $1.5 \times 10^{20} \text{ cm}^{-3}$ . For the multigroup calculations we have divided the frequency range into 1, 10, 30 and 100 homogeneous (equally spaced in energy) groups. The Planck mean is mainly ruled by the strength of the absorption peaks whereas Rosseland is an harmonic mean which gives greatest weight to the more transparent regions of the spectrum. For these reasons, the Planck group means try to reproduce the peaks of the monochromatic spectrum and the Rosseland ones better suit the absorption valleys, as is well illustrated, for example, in the photon energy range 40–55 eV of Fig. 10(a) and (b) and in Fig. 10(c) and (d) in which are represented comparisons of the monochromatic opacities and Planck and Rosseland group means for a temperature of 630 eV and electron density of  $1.6 \times 10^{14} \text{ cm}^{-3}$ .

From Fig. 10(a) and (b) we detect that for the range of photon energies higher than 80 eV, even the simulation including only 10 groups provide close values of the group opacities to those obtained with larger number groups and the simulation including 30 groups already presents a quite reasonable agreement with the monochromatic spectrum in that range. The smooth variation with the photon energy of the monochromatic opacity indicates that it is not necessary to include many groups in that range. On the other hand, in the photon energy range 40–80 eV, where the opacity shows strong variations with the photon frequency, greater differences are obtained as a function of the number of groups considered in the simulations, overall for the group Planck mean which is more sensitive to the strength of the absorption peaks. We observe that, although the simulation including 100 groups provides a general agreement to the monochromatic spectrum, the height of several peaks (as for example, those located at photon energies around 15, 30, 40 and 50 eV) are not reproduced in the Planck group opacity. These are very narrow peaks, so an increase in the number of groups should be required to obtain a better representation of them. However, as said before, a compromise between accuracy and computational cost must be achieved and, then, any further increase in the number of the groups should be taken carefully. Obviously, another choice is to divide the photon frequency range into non-homogeneous groups including a greater number of groups in the regions where the spectrum presents a stronger dependence with the photon frequency than in the regions where that dependence is smoother. This option is very useful when the major features of the spectrum are spanned over wide range of photon energies, as is the case when the electron temperature increases.

Fig. 10(c) and (d) displays a comparison among the monochromatic and multigroup opacities obtained following that premise. In this case, the electron temperature is 630 eV and there are more heavier elements that contribute to the opacity (such as Mg, Si, S and Fe) than at the temperature of 10 eV and this is why the spectrum is significantly more complex than for the former temperature. This issue along with the fact that those elements that were present at 10 eV are more ionized at this higher temperature mean that the spectrum spans over a larger range of photon energies. Therefore, in order to obtain a reasonable agreement, the number of groups were increased with respect to the case of temperature of 10 eV. However, since the complexity of the spectrum is mainly located for photon energies lower than around 3000 eV, we performed calculations including either 180 or 250 groups for energies up to 3000 eV and only 20 groups for the greater photon energies range, where the spectrum presents a smoother behavior with the frequency (for clarity, the figure only shows energies up to 5000 eV). Figures show that 20 groups are enough to provide an acceptable reproduction of the spectrum for the range of energies higher than 3000 eV. On the other hand, for range of photon energies lower than 3000 eV we detect for the group Planck opac-

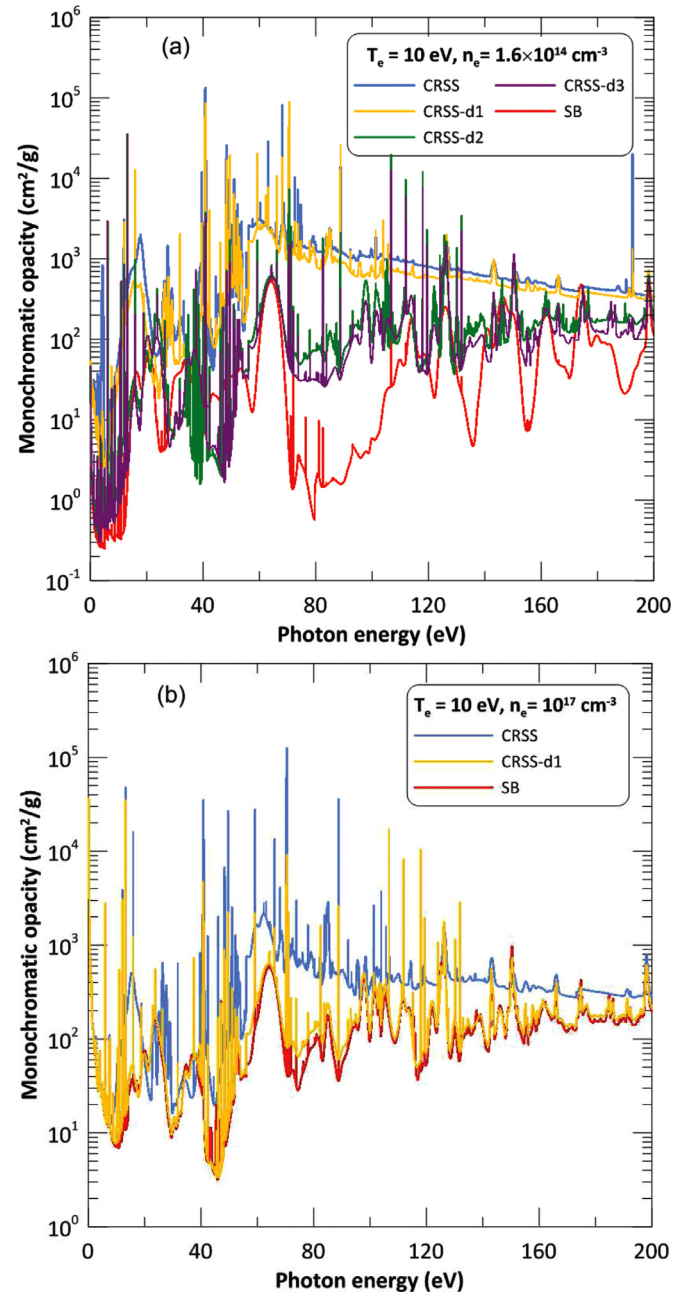


Fig. 11. Comparison of the monochromatic opacities calculated assuming the plasma as optically thin (CRSS), including self-absorption and in LTE regime (SB).

ity that the 180 and 250 groups calculations reproduce in a rather similar manner the monochromatic spectrum although the simulation performed with 250 groups provides slight better estimations of the strength of the peaks. With the number of groups considered, both multigroup simulations reproduce most of the peaks of the spectrum although differences around one order of magnitude are found. This could be due to the fact that in the range 0–1500 eV the opacity is a widely varying function of frequency and in the range of energies 1500–3000 we have isolated narrow lines associated with the contributions of the He-like and H-like ions of magnesium, silicon and sulfur. Due to this fact and also that the group Rosseland mean is more influenced by the depth of the valleys in the absorption spectrum, we observe in the figures that this mean reproduces, on average, those valleys in the monochromatic opacity.



**Table 1**

Comparison of the average ionizations for the most relevant elements at the electron temperature of 10 eV and two electron densities:  $n_{e1} = 1.6 \times 10^{14}$  and  $n_{e2} = 10^{17} \text{ cm}^{-3}$ . The calculations were performed using the SB and the optically thin and thick CRSS models.

	N		O		Ne	
	$n_{e1}$	$n_{e2}$	$n_{e1}$	$n_{e2}$	$n_{e1}$	$n_{e2}$
CRSS	3.0	4.0	2.9	4.0	2.9	3.5
CRSSd1	3.6	4.9	3.7	5.1	3.0	4.8
CRSSd2	4.9	4.9	5.0	5.2	4.9	4.9
CRSSd3	5.0	5.0	5.5	5.2	5.5	4.9
SB	5.0	5.0	6.0	5.3	6.5	4.9

For the reasons above commented, a better reproduction of the features in the range of energies up to 3000 eV would entail a considerable increase of the number of the groups with the consequent rise of the computational costs. In either case, the multi-group simulations with the number of groups considered provide significantly better results than the gray (or one-group) approach, which is widely used. To illustrate that, we have also included in the representations the Planck and Rosseland mean opacities in order to show the differences with respect to the monochromatic and multigroup opacities. One-group (gray) opacities strongly depends on the weighting function. This function reaches its maximum at the photon energies of  $2.8T_e$  and  $3.8T_e$  eV for the Planck and Rosseland means, respectively. Therefore, the mean opacities will be mainly ruled by the absorption features which are located in a range of photon energies near these maximum. The chemical elements included in the multicomponent plasma under analysis contribute in different ranges of photon energies. Therefore, for a given plasma condition, the mean opacity could be mainly due to some of the elements of the mixture that contribute in that photon energy range. Thus, at 10 eV, the Planck and Rosseland weight functions peak at the photon energies of 28 and 38 eV, respectively. Therefore, the Planck means will be mainly influenced by the absorption peaks in the energy range around 10–50 eV, overestimating the opacity, with respect to the monochromatic and group opacities, even one order of magnitude for photon energies ranged from around 20 to 40 eV and in the range of photon energies greater than 80 eV, as Fig. 10(a) shows and underestimates, for example, the continuum edge of  $\text{He}^{+1}$  ion, that the multigroup approach reproduces quite well. On the other hand, at this temperature the Rosseland mean will be mainly ruled by the contributions in range of photon energies around 20–70 eV and, for this reason, it predicts a considerably lower value of the opacity respect to the multigroup one, for the photon energy ranges lower than 20 eV and from 60 to 80 eV and overpredicts the opacity for higher energies, see Fig. 10(b).

As the electron temperature increases, since the number of elements that contribute to the opacity is greater and the spectrum is more complex, the differences obtained might be more important. For the electron temperature of 630 eV, the Planck and Rosseland means peak at 1764 and 2394 eV, respectively. Therefore, the peaks that most contribute to the Planck mean would be those associated to the transitions of the He-like and H-like Mg and Si ions according to Fig. 8(a), although we see from that figure that the iron contribution to the absorption spectrum is significant, for example. As a consequence, the Planck mean opacity overpredicts the absorption for photon energies higher than 3500 eV, which is well reproduced by the multigroup opacity, see Fig. 10(c). Furthermore, the differences in the heights of the absorption peaks in the range of photon energies 700–2500 eV are, in general, around one order of magnitude, reaching the two orders in several features, whereas

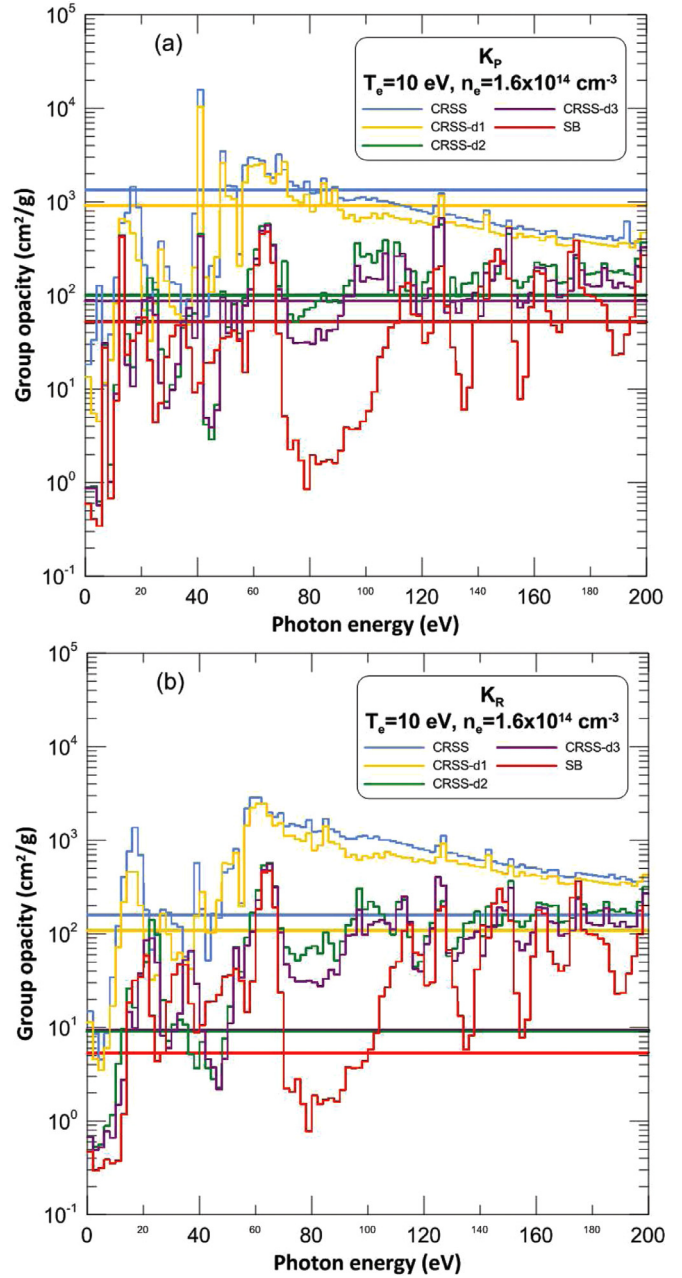


**Fig. 12.** Comparison of (a) Planck and (b) Rosseland multigroup and mean opacities calculated using CRSS optically thin and thick models and SB model.

these differences are considerably reduced in the multigroup calculations. For the Rosseland mean case, as the maximum of the function is shifted towards higher energies, this opacity is mainly ruled by the contributions of the He-like and H-like Si and S ions. As a consequence, its reproduction of the depth of the valleys of the monochromatic opacity is considerably worse than the multigroup simulations, as Fig. 10(d) shows.

### 3.3. Analysis of the effect of plasma self-absorption in the monochromatic and multigroup opacities

In the previous section the study of the opacities was made assuming the plasma to be optically thin. However, there are situations in which the self-absorption of the plasma radiation becomes relevant due to the dimensions of the plasma. In this case, both the atomic kinetics and the opacities could be modified with re-



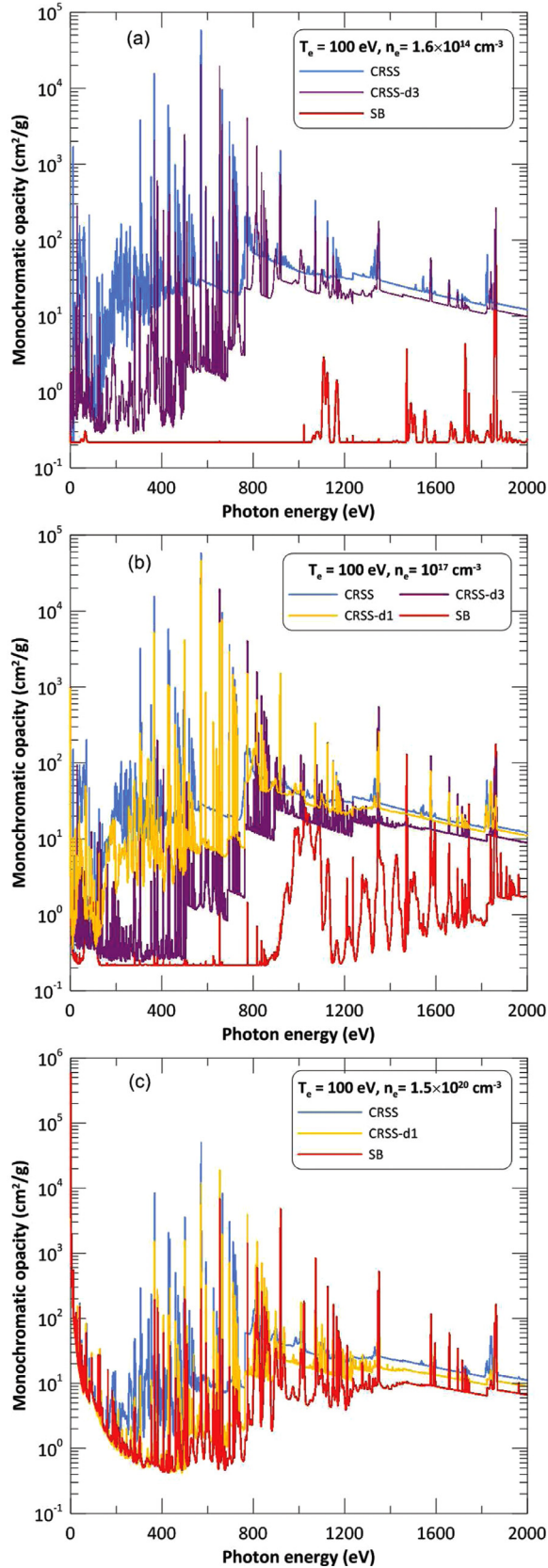


**Fig. 13.** Comparison of the monochromatic opacities calculated assuming the plasma as optically thin (CRSS) and thick (CRSS-d) and in LTE regime (SB).

spect to the results obtained in the optically thin NLTE simulations. This section is devoted to the analysis of the influence of the radiation trapping in the calculation of the plasma radiative opacities and also of the departures from LTE regime. As mentioned before, plasma self-absorption are included in MIXKIP by means of the escape factor formalism. For the analysis, we have considered the plasma with planar geometry and three values for the plasma slab width,  $d_1 = 10^2$  m,  $d_2 = 10^7$  m and  $d_3 = 10^{12}$  m. For fixed plasma conditions, the increase of plasma width in the NLTE calculations tends to approximate the average ionization, plasma level populations and radiative properties to those obtained in LTE simulations. The optical depth rises with the plasma geometrical dimension and this fact makes that the probability that the photon thermalizes before it escapes approaches unity [5]. When this occurs for any photon frequency the source function tends to the Planck function which is the one obtained in LTE regime.

As is generally known, the LTE regime is enhanced as the electron temperature decreases and the electron density increases since in both situations the relative importance of the collisional processes in the plasma is reinforced. When the plasma is out of this thermodynamic regime, Saha-Boltzmann (SB) simulations overpredict the average ionization with respect to CRSS simulations. As a consequence, the absorption spectra will be shifted towards higher photon energies and the values of the opacities provided by the SB simulations will be lower than those obtained from the CRSS model. The plasma self-absorption produces an increase of the population in the atomic excited configurations which may undergo a subsequent ionization due to other atomic processes and, then, the average ionization rises with respect to the optically thin situation. Therefore, the average ionizations and the monochromatic opacities, predicted by the CRSS optically thick simulations, will be scored between those obtained with the optically thin and SB models.

As said before, the plasma analyzed in this work involves chemical elements that can have very different ionization potentials. Hence, for a given plasma condition, the atomic structure of the ions present in the plasma, and hence also the influence of the radiation trapping on them, may be quite different. Thus, for example, we can find situations in which some of the chemical elements have a closed-shell ion configuration and therefore the effect of the radiation trapping might be significantly lower than for ions of other chemical elements with open-shell configurations. This fact would imply that the optically thick absorption spectra could be more similar to those obtained in the optically thin approach in those photon energy ranges where the former ions are the main contributors.

To illustrate this, we have represented in Fig. 11(a) and (b) the comparison of the monochromatic opacities of the plasma mixture calculated in NLTE both in optically thin (CRSS) and thick approaches (denoted as CRSS-d1, -d2 and -d3, for the three slab widths, respectively) and in LTE (SB) for a plasma temperature of 10 eV and electron densities of  $1.6 \times 10^{14}$  and  $10^{17}$  cm<sup>-3</sup>, respectively. According to the previous analysis, the most contributing elements at this temperature are carbon, nitrogen and oxygen and, for the lower density, helium is relevant as well.

For the lower density represented (Fig. 11(a)), the effect of the self-absorption in the monochromatic opacity is significant for the two largest slab widths considered (CRSS-d2 and CRSS-d3), whereas for the lowest width (CRSS-d1) the spectrum is quite similar to that of the optically thin situation (CRSS), including the same features although with lower strength. Both the optically thin and thick simulations predict a value of 2 for the helium average ionization. However, the fractional abundance of the He<sup>+</sup> ion (which is the responsible for the helium line contribution to the total spectrum) obtained with the CRSS and CRSS-d1 models

are quite similar, 0.29 and 0.19, respectively, whereas CRSS-d2 and CRSS-d3 models provide values around  $8.0 \times 10^{-4}$ .

This considerable drop is partly responsible of the reduction of the monochromatic opacity in the range of photon energies 40–50 eV and for energies higher than 80 eV. Something similar occurs with carbon. Although all the models predict an average ionization around 4, CRSS and CRSS-d1 predict similar fractional abundances for  $C^{+3}$  and  $C^{+4}$  ions (0.13, 0.27 and 0.87, 0.72, respectively) whereas the other two optically thick cases provide values of  $C^{+4}$  close to one. The effects of the radiation trapping are more relevant for nitrogen, oxygen and neon. In Table 1 are listed the values of the average ionization obtained with the different models. Slight differences are detected for nitrogen and oxygen between the CRSS and CRSS-d1 model. However, both predict a similar set of relevant ions for these elements at this plasma condition, although with slight differences in their abundances, which may explain why the spectra of both models include the same structures but with different strengths. On the other hand, the increases of the average ionizations in these elements are more noticeable as the slab width increases and this contributes to the reduction of the opacity observed in the figure. We also detect that for oxygen and neon, when the width is increased from  $d_2$  to  $d_3$ , their average ionization rises around 0.5 and the differences in these elements are the responsible for the changes between CRSS-d2 and CRSS-d3 spectra, due to the average ionization of nitrogen does not change since its most abundant ion is  $N^{+5}$ , i.e. a closed-shell configuration ion. As said before, the effect of the self-absorption will depend on the chemical element.

When the density increases to  $10^{17} \text{ cm}^{-3}$ , the absorption coefficient of the elements increase and then the optical depth. Thus, Fig. 11(b) and Table 1 show that the differences between the CRSS and CRSS-d1 calculations are more important than for the lower density. In the figure, for the optically thick cases, only the CRSS-d1 spectrum has been represented. This is due to, at this density, the three optically thick spectra are quite similar. In the table we can observe that the three models provide rather similar average ionizations. The increase of absorption coefficient reduces the photon mean free path and its value will be around the lowest value of the slab width, i.e.  $10^2 \text{ m}$  and, therefore, an increase of the plasma width will not result in greater values of the average ionization of the elements.

LTE regime is achieved as the electron density increases since this encourages the relevance of the collisional processes in the plasma. Thus, at this temperature we have obtained that the former regime can be assumed for an electron density of around  $10^{19} \text{ cm}^{-3}$ . Above this density the radiation trapping will not have effects in the plasma microscopic properties. For the density of  $10^{17} \text{ cm}^{-3}$ , the optically thick spectra are closer to the SB than to the CRSS one. Therefore, the greater discrepancies between the thick models CRSS-d2 and CRSS-d3 and SB are obtained for the lowest density analyzed as Fig. 11(a) and Table 1 show.

On the other hand, we have also analyzed the low density limit considered in this work, i.e.  $10^{11} \text{ cm}^{-3}$ , obtaining that, for this

density, the effects of the self-absorption becomes relevant for the largest slab width considered only.

The differences obtained for the monochromatic opacities have their direct correlation to the multigroup and mean opacities. In Figs. 12(a) and (b) we have displayed the comparison of group Planck and Rosseland opacities, respectively, considering 1 and 100 homogeneous frequency groups, calculated using the CRSS optically thin and thick and the SB models at the electron temperature of 10 eV and for the lowest density. As for the monochromatic opacities, the group opacities obtained from CRSS and CRSS-d1 present some differences although they are always of the same order of magnitude. On the other hand, the differences between the CRSS and CRSS-d2 and CRSS-d3 are greater and for some photon energy ranges they can reach one order of magnitude, as for example for energies lower than 80 eV, both for the Planck and Rosseland group opacities. This result is expected according to the results obtained for the monochromatic opacities. Differences of one order of magnitude are also found for the opacities in the gray approach. From the figures we observe that the CRSS-d2 and CRSS-d3 Planck and Rosseland mean opacities are quite similar. However, for the group opacities we observe relative differences around 100% between them for some photon energy regions, as for example 80–110 eV, which agrees with the situation observed for the monochromatic opacities. Therefore, the influence of the weighting function in the gray approach may lead to inappropriate results. The differences between the CRSS and SB simulations of the group opacities may reach even two or three orders of magnitude. However, when the radiation trapping is taking into account due to the plasma dimensions, the differences between the results obtained with the CRSS-d2 and CRSS-d3 and SB models are reduced considerably with respect to the other two models. In this case, the maximum discrepancies are around one order of magnitude although the differences are lower in general. As regards the mean opacities, the CRSS-d2 and CRSS-d3 results are around twice greater than those of the SB. The differences are still large but significantly smaller than those obtained between the SB and CRSS models. So, SB approach is not accurate enough, but is not the CRSS model for the two larger slab widths either and, therefore, the corresponding optically thick models should be used in these situations.

For a given slab width and electron density, an increase of electron temperature will result in a reduction of the absorption coefficient of the elements and, therefore, of the optical depth. Thus, at the electron temperature of 100 eV and for the electron density of  $1.6 \times 10^{14} \text{ cm}^{-3}$  the effect of the self-absorption in the total opacity is only significant for the largest slab width. In Fig. 13(a), its spectrum is compared with those of the optically thin and SB models. At this temperature, the most relevant elements are C, N, O, Mg, Si, S and Fe, although the latter has a larger contribution for the two greatest densities considered. As commented before, the effect of the self-absorption depends on the chemical element and its ionization stage for a given plasma condition. At the temperature of 100 eV, and for the three densities, carbon and nitrogen have average ionizations around 5.5 and, therefore, the changes due to the radiation trapping are not significant. The most abun-

**Table 2**

Comparison of the average ionizations for nitrogen, oxygen, silicon, sulfur and iron at the electron temperature of 100 eV and three electron densities:  $n_{e1} = 1.6 \times 10^{14}$ ,  $n_{e2} = 10^{17}$  and  $n_{e3} = 1.5 \times 10^{20} \text{ cm}^{-3}$ . The calculations were performed using the SB and the optically thin and thick CRSS models.

	N			O			Si			S			Fe		
	$n_{e1}$	$n_{e2}$	$n_{e3}$	$n_{e1}$	$n_{e2}$	$n_{e3}$	$n_{e1}$	$n_{e2}$	$n_{e3}$	$n_{e1}$	$n_{e2}$	$n_{e3}$	$n_{e1}$	$n_{e2}$	$n_{e3}$
CRSS	5.3	5.3	5.7	5.4	5.4	5.8	8.9	9.3	11.2	8.8	9.0	11.4	11.6	11.9	15.5
CRSSd1	5.3	5.8	5.9	5.4	6.0	6.6	8.9	10.3	11.9	8.8	10.0	13.6	11.7	13.8	16.3
CRSSd2	5.3	5.9	5.9	5.5	6.7	6.6	9.7	11.9	11.9	9.2	12.1	13.6	12.6	15.7	16.3
CRSSd3	5.9	5.9	5.9	6.5	6.7	6.6	10.5	12.0	11.9	10.6	13.5	13.6	14.2	16.0	16.3
SB	6.0	6.0	6.0	7.0	7.0	6.9	12.7	12.0	11.9	14.0	14.0	13.8	23.9	21.0	16.5

dant ion for neon and magnesium, for the three densities, is the He-like one, a closed-shell ion, and their average ionization do not change with the self-absorption. The elements more affected are oxygen, silicon, sulfur and iron and their average ionizations are listed in Table 2. The table shows that, for the electron density of  $1.6 \times 10^{14} \text{ cm}^{-3}$ , there are appreciable variations for the largest slab width only. We have checked that if the density is decreased to  $10^{11} \text{ cm}^{-3}$  (very low density limit) the effects of the radiation trapping for the largest slab width are not too relevant and, therefore, for temperatures greater than 100 eV and that density, the plasma can be considered as optically thin.

When the density increases to  $10^{17} \text{ cm}^{-3}$ , the photon mean free path decreases and now there are differences for the lowest slab width, as Fig. 13(b) shows. In the figure the spectrum obtained

with the CRSS-d2 model is not represented, since this is quite similar to that of the CRSS-d3 model. Table 2 also shows that the average ionizations predicted by both models at this density for all the relevant elements are rather similar and they are also close to the LTE values, except for the sulfur and iron cases. With respect to the CRSS model, the elements that present more differences are oxygen, silicon, sulfur and iron and, for this reason, the main discrepancies in the spectra are located in the region of photon energies lower than 700 eV. This also occurs for the density of  $1.6 \times 10^{14} \text{ cm}^{-3}$ .

Finally, for the electron density of  $1.5 \times 10^{20} \text{ cm}^{-3}$ , the average ionizations of all the elements obtained from the optically thick simulations are nearly identical of the values predicted by the SB model. Therefore, at this density, the photon mean free path will

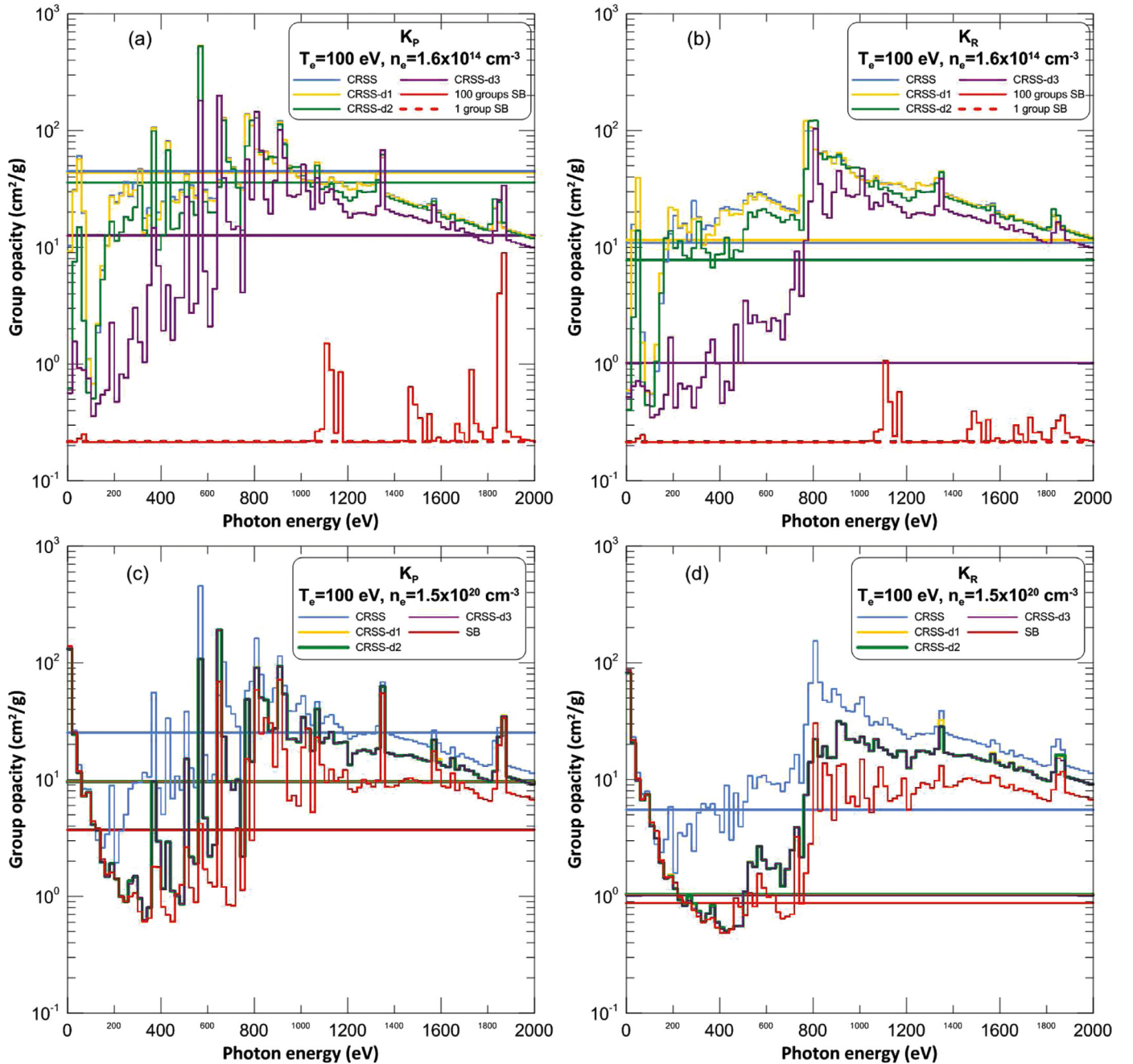


Fig. 14. Comparison of Planck (figures (a) and (c)) and Rosseland (figures (b) and (d)) multigroup and mean opacities calculated using CRSS optically thin and thick models and SB model.



be of the same order of  $d_1$  and, for this reason, subsequent increases of the slab width does not produce further effects. Therefore, the optically thick and SB spectra present similar structures (see Fig. 13(c)) although there are differences in their strength due to disagreements in the fractional abundances of the plasma levels in both models. As the electron temperature grows above 100 eV the effect of the self-absorption will be reduced.

We had obtained that at the electron temperature of 10 eV and electron density of  $1.5 \times 10^{20} \text{ cm}^{-3}$ , the plasma can be assumed in LTE. However, at 100 eV, Fig. 13(c) shows that, although the CRSS and SB spectra are more similar for that density than for the other two lower ones, there are still some differences between them. The increase of the temperature diminishes the relative importance of the collisional processes and for this reason, if we assume the plasma as optically thin, for electron temperatures greater than or equal to 100 eV, the achievement of the LTE regime will require greater densities. On the other hand, for this density, the effects of the radiation trapping make the spectra of the SB and optically thick models more similar.

Fig. 14(a) and (b) display the comparison of Planck and Rosseland group opacities at the electron temperature of 100 eV and for the electron density of  $1.6 \times 10^{14} \text{ cm}^{-3}$ , respectively, considering 1 and 100 homogeneous frequency groups, calculated using the CRSS optically thin and thick and SB models. As was obtained for the monochromatic opacities, CRSS and CRSS-d1 multigroup opacities are rather similar, the CRSS-d2 ones present slight differences, overall in the range of photon energies lesser than 300 eV, and great discrepancies are obtained for the CRSS-d3 multigroup opacities that can reach one order of magnitude for photon energies lower than 700 eV. Therefore, for this plasma width the radiation trapping should be included in the atomic kinetics calculations. With respect to the LTE simulation, large disagreements are obtained in almost the whole range of photon energies that can even reach three orders of magnitude. Regarding the mean opacities, the influence of the weighting functions, which reach their maximum at 280 and 380 eV for the Planck and Rosseland means, respectively, is detected. Thus, for the CRSS-d3 model, the Planck and Rosseland means predict significantly small values of the opacities in the ranges of energy around 600–1400 eV and 400–2000 eV, respectively. This underestimation also occurs for the LTE simulation.

When the density increases to  $1.5 \times 10^{20} \text{ cm}^{-3}$ , the three optically thick models provide the same multigroup and mean opacities, which agrees with the results obtained for the monochromatic opacities. In this case, the optically thick spectra are, in general, closer to the LTE spectrum than to the optically thin one, for photon energies lower than 700 eV. With respect to the mean opacities, for the Rosseland case, the optically thick and LTE results are quite similar, due to the influence of weighting function that reaches its maximum in a photon energy range in which both monochromatic opacities are rather similar. The differences are slightly greater for the Planck mean opacity although the differences are of the same order of magnitude. As for the lower density, we observe that the mean opacities underestimate the values of the opacity in wide ranges of photon energies.

These differences between the optically thin and optically thick models will be reduced as the electron temperature increases since the self-absorption becomes less relevant. On the other hand, for the electron density of  $10^{11} \text{ cm}^{-3}$  the effect of the self-absorption is appreciable for the largest slab width and for low electron temperatures (up to around 10 eV).

#### 4. Conclusions

Radiation-hydrodynamic simulations require of quantities that involve integrals of the specific intensity over the frequency variable. These quantities are obtained from the resolution of the ra-

diative transfer equation which requires the calculation of radiative opacities. In this work we have carried out calculations of the monochromatic, multigroup and mean opacities of an astrophysical plasma mixture for electron temperatures and densities ranging from 1 to 1000 eV and  $10^{11}$  to  $1.5 \times 10^{20} \text{ cm}^{-3}$ , respectively, which cover situations of NLTE and LTE thermodynamic regimes. Since the mixture includes chemical elements with different ionization potentials, we have performed an analysis of the relative importance of their contribution to the total monochromatic opacity as a function of the electron density and temperature of the plasma. Furthermore, the elements will contribute at different regions of photon energies in the absorption spectra. For the calculations of the plasma level populations and monochromatic opacities a collisional-radiative model was used assuming the plasma as homogeneous in steady state and optically thin. We have found that the relevance of hydrogen and helium is mainly for electron temperatures lower than 50 eV. Carbon, nitrogen, oxygen and neon also starts contributing at low temperatures. For temperatures higher than 100 eV, the carbon and nitrogen contribution will be mainly due to their H-like ion, whereas this will occur for oxygen and neon for temperatures greater than 300 eV. The contribution of magnesium, silicon and sulfur becomes appreciable at the electron temperature of 50 eV and the iron contribution begins to be noticeable at the electron temperature of 100 eV. The influence of the density in the contribution of the different chemical elements is less important than the influence of the temperature.

Since the resolution of the RTE for each frequency in radiation-hydrodynamic simulations entails high computational costs, the multigroup method is a commonly used method for handling the frequency variables in the RTE in order to achieve a compromise between accuracy and computational costs. In this work we have made an analysis of the influence of the number of the groups used in the Planck and Rosseland multigroup opacity simulations. The radiative opacities of the multicomponent plasma analyzed are, in general, widely varying functions of the frequency. When a low number of groups is considered in the multigroup method, the influence of the weighting functions is significant and this may lead to inappropriate results, especially in the gray approach. For the range of temperatures analyzed, as the temperature increases the complexity of the absorption spectra spans over larger range of photon energies. This might entail the increase of the number of groups, but an alternative option to avoid that is to divide the photon frequency range into non-homogeneous groups including more of them in those range of photon energies where the opacity presents a greater dependence on frequency and a few number of groups where the opacity shows a smooth behavior with the frequency.

We also presented results about the influence of the plasma self-absorption in the monochromatic and multigroup opacities of the plasma mixture assuming planar geometry and the departures from LTE regime. The study was made for three slab widths, for two temperatures and for three densities. As the plasma mixture includes chemical elements that may have quite different ionization potentials, the effect of the radiation trapping, for a given plasma condition, will not be the same and this fact will have a direct effect on the absorption spectrum. The effect of the self-absorption decreases as the electron density drops and also with an increase of the electron temperature. In both cases, the absorption coefficient diminishes and then the effect of the radiation trapping. Thus, for the electron density of  $10^{11} \text{ cm}^{-3}$  the effect of the self-absorption is appreciable for electron temperatures lower than 10 eV and for the largest slab width considered. On the other hand, in the range of electron densities  $10^{14} - 10^{20} \text{ cm}^{-3}$  and depending on the electron temperature, the optically thick simulations may produce quite different results to those of the optically thin model and, therefore, in these cases self-absorption effects



should be considered. For the low electron temperatures regime (up to around 50 eV), we obtained the LTE thermodynamic regime can be assumed for the electron density of  $10^{19} \text{ cm}^{-3}$ . On the other hand, as the temperature increases, the threshold value for the density also does and we detected that at 100 eV the value required to assume the plasma to be in LTE is higher than  $10^{20} \text{ cm}^{-3}$ . However, there are situations in which the optically thick results are closer to those obtained assuming the plasma in LTE than those provided by optically thin calculations.

## Acknowledgments

This work was supported by the Spanish Government through Project No. FIS2016-81019-P.

## Supplementary material

Supplementary material associated with this article can be found, in the online version, at doi:[10.1016/j.jqsrt.2019.106633](https://doi.org/10.1016/j.jqsrt.2019.106633).

## References

- [1] Jin F, Zeng J, Yuan J, Han G, Wu Z, Yan J, et al. L to m shell transitions and model comparisons for radiative opacities of sodium fluoride plasma. *J Quant Spectrosc Radiat Transfer* 2005;95:241–53.
- [2] Pradhan A, Nahar S. *Atomic astrophysics and spectroscopy*. New York: Cambridge University Press; 2011.
- [3] Bailey J, Roachau G, Mancini R, Iglesias C, Macfarlane J, Golovkin I, et al. Experimental investigation of opacity models for stellar interior, inertial fusion, and high energy density plasmas. *Phys Plasmas* 2009;16:058101.
- [4] Drake R. Theory of radiative shocks in optically thick media. *Phys Plasmas* 2007;14:043301.
- [5] Mihalas D, Weible-Mihalas B. *Foundations of radiation hydrodynamics*. New York: Dover Publications Inc.; 1999.
- [6] Pomraning G. *The equations of radiation hydrodynamics*. New York: Dover Publications; 1973.
- [7] Rogers F, Iglesias C. Radiative atomic Rosseland mean opacity tables. *Astrophys J Sup Ser* 1992;79:507–68.
- [8] Iglesias C, Rogers F. Updated OPAL opacities. *Astrophys J* 1996;464:943–53.
- [9] Seaton M, Yan Y, Mihalas D, Pradhan A. Opacities for stellar envelopes. *Mon Not R Astron Soc* 1994;266:805–28.
- [10] Seaton M, Badnell N. A comparison of Rosseland-mean opacities from OP and OPAL. *Mon Not R Astron Soc* 2004;354:457–65.
- [11] Badnell N, Bautista M, Butler K. Updated opacities from the opacity project. *Mon Not R Astron Soc* 2005;360:458–64.
- [12] Blancard C, Cosse P, Faussurier G. Solar mixture opacity calculations using detailed configuration and level accounting treatments. *Astrophys J* 2012;754:10.
- [13] Colgan J, Kilcrease D, Magee N, Sherrill M, Abdallah J, Hakel P, et al. A new generation of los alamos opacity tables. *Astrophys J* 2016;817:116.
- [14] Salzmänn D. *Atomic physics in hot plasmas*. New York: Oxford University Press; 1998.
- [15] Bates R, Kingston A, McWether R. Recombination between electrons and atomic ions, I. optically thin plasmas. *Proc R Soc London Ser-A* 1962;267:297–312.
- [16] Scott H, Hansen S. Advances in NLTE modeling for integrated simulations. *High Energy Density Phys* 2010;6:39–47.
- [17] Bauche J, Bauche-Arnoult C, Klapisch M. Transition arrays in the spectra of ionized atoms. *Adv At Mol Phys* 1987;23:131–95.
- [18] Bar-Shalom A, Oreg J, Goldstein W, Shvarts D, Zigler A. Super-transition-arrays. a model for the spectral-analysis of hot, dense-plasma. *Phys Rev A* 1989;40:3183–93.
- [19] Mazevet S, Abdallah J. Mixed UTA and detailed line treatment for mid-Z opacity and spectral calculations. *J Phys B* 2006;39:3419–29.
- [20] Hansen S, Bauche J, Bauche-Arnoult C, Gu M. Hybrid atomic models for spectroscopic plasma diagnostics. *High Energy Density Phys* 2007;3:109–14.
- [21] Hansen S, Fontes C, Colgan J, Abdallah J, Chung H, Scott H, et al. Modern methods in collisional-radiative modeling of plasmas. Berlin: Springer; 2016.
- [22] Rodríguez R, Espinosa G, Gil J. Radiative properties for astrophysical plasma mixtures in nonlocal thermodynamic equilibrium. *Phys Rev E* 2018;98:033213.
- [23] Schure K, Kosenko D, Kaastra J, Keppens R, Vink J. A new radiative cooling curve based on an up-to-date plasma emission code. *Astron Astrophys* 2009;508:751–240.
- [24] Bradshaw S, Cargill P. The cooling of coronal plasmas - II. properties of the radiative phase. *Astron Astrophys* 2005;437:311–17.
- [25] Gnat O, Sternberg A. Time-dependent ionization in radiatively cooling gas. *Astrophys J Sup Ser* 2007;168:213–30.
- [26] Sacco G, Orlando S, Argiroffi C, Maggio A, Peres G, Reale F, et al. On the observability of t tauri accretion shocks in the X-ray band. *Astron Astrophys* 2010;522:A55.
- [27] Asplund M, Grevesse V, Sauval A, Scott P. The chemical composition of the sun. *Annu Rev Astron Astrophys* 2009;47:481–522.
- [28] Gu M. The flexible atomic code. *Can J Phys* 2008;86:675–89.
- [29] Lotz W. Electron-impact ionization cross-sections and ionization rate coefficients for atoms and ions from hydrogen to calcium. *Z Phys* 1968;216:241–7.
- [30] Vanregemorter H. Rate of collisional excitation in stellar atmospheres. *Astrophys J* 1962;136:906–15.
- [31] Kramers H. On the theory of X-ray absorption and of the continuous X-ray spectrum. *Philos Mag* 1923;46:836–71.
- [32] Griem H. *Principles of plasma spectroscopy*. Cambridge: Cambridge University Press; 1997.
- [33] Abdallah JJ, Colgan J, Rohringer N. Time-dependent calculations of electron energy distribution functions for neon gas in the presence of intense xfel radiation. *J Phys B* 2013;46:235004.
- [34] Mancini R, Orlando R, Hooper C. Escape factors for stark-broadened line-profiles. *J Phys B* 1987;20:2975–87.
- [35] Stewart J, Pyatt K. Lowering of ionization potentials in plasmas. *Astrophys J* 1966;144:1203–11.
- [36] Rodríguez R, Florido R, Gil J, Rubiano J, Martel P, Minguez E. RAPCAL Code: a flexible package to compute radiative properties for optically thin and thick low and high-z plasmas in a wide range of density and temperature. *Laser Part Beams* 2008;26:433–48.
- [37] Rodríguez R, Florido R, Gil J, Rubiano J, Suarez D, Martel P, et al. Collisional-radiative calculations of optically thin and thick plasmas using the computational package ABAKO/RAPCAL. *Commun Comput Phys* 2010;8:185–210.
- [38] Dimitrijevic M, Konjevic N. Simple estimates for stark-broadening of ion lines in stellar plasmas. *Astron Astrophys* 1987;172:345–9.
- [39] Rose S. Calculations of the radiative opacity of laser-produced plasmas. *J Phys B* 1992;25:1667–81.
- [40] Rutten R. *Radiative Transfer in Stellar Atmospheres*. Utrecht: Sterrekundig Instituut Utrecht; 1995.
- [41] Espinosa G, Rodríguez R, Gil J, Suzuki-Vidal F, Lebedev S, Ciardi A, et al. Influence of atomic kinetics in the simulation of plasma microscopic properties and thermal instabilities for radiative bow shock experiments. *Phys Rev E* 2017;95:033201.